NASA/TM–2018-219807

Finite Element Simulations of Two Vertical Drop Tests of F-28 Fuselage Sections

Karen E. Jackson, Justin D. Littell, Martin S. Annett, and Ian M. Haskin
Langley Research Center, Hampton, Virginia

February 2018

NASA STI Program . . . in Profile

Since its founding, NASA has been dedicated to the advancement of aeronautics and space science. The NASA scientific and technical information (STI) program plays a key part in helping NASA maintain this important role.

The NASA STI program operates under the auspices of the Agency Chief Information Officer. It collects, organizes, provides for archiving, and disseminates NASA's STI. The NASA STI program provides access to the NTRS Registered and its public interface, the NASA Technical Reports Server, thus providing one of the largest collections of aeronautical and space science STI in the world. Results are published in both non-NASA channels and by NASA in the NASA STI Report Series, which includes the following report types:

- TECHNICAL PUBLICATION. Reports of completed research or a major significant phase of research that present the results of NASA Programs and include extensive data or theoretical analysis. Includes compilations of significant scientific and technical data and information deemed to be of continuing reference value. NASA counter-part of peer-reviewed formal professional papers but has less stringent limitations on manuscript length and extent of graphic presentations.

- TECHNICAL MEMORANDUM. Scientific and technical findings that are preliminary or of specialized interest, e.g., quick release reports, working papers, and bibliographies that contain minimal annotation. Does not contain extensive analysis.

- CONTRACTOR REPORT. Scientific and technical findings by NASA-sponsored contractors and grantees.

- CONFERENCE PUBLICATION. Collected papers from scientific and technical conferences, symposia, seminars, or other meetings sponsored or co-sponsored by NASA.

- SPECIAL PUBLICATION. Scientific, technical, or historical information from NASA programs, projects, and missions, often concerned with subjects having substantial public interest.

- TECHNICAL TRANSLATION. English-language translations of foreign scientific and technical material pertinent to NASA's mission.

Specialized services also include organizing and publishing research results, distributing specialized research announcements and feeds, providing information desk and personal search support, and enabling data exchange services.

For more information about the NASA STI program, see the following:

- Access the NASA STI program home page at http://www.sti.nasa.gov

- E-mail your question to help@sti.nasa.gov

- Phone the NASA STI Information Desk at 757-864-9658

- Write to:
  NASA STI Information Desk
  Mail Stop 148
  NASA Langley Research Center
  Hampton, VA 23681-2199

NASA/TM–2018-219807

Finite Element Simulations of Two Vertical Drop Tests of F-28 Fuselage Sections

Karen E. Jackson, Justin D. Littell, Martin S. Annett, and Ian M. Haskin
Langley Research Center, Hampton, Virginia

National Aeronautics and
Space Administration

Langley Research Center
Hampton, Virginia 23681-2199

February 2018

Available from:

NASA STI Program / Mail Stop 148
NASA Langley Research Center
Hampton, VA 23681-2199
Fax: 757-864-6500

Table of Contents

List of Figures

List of Figures (Continued)

List of Figures (Continued)

Page

List of Figures (Concluded)

Page

List of Tables

List of Acronyms

ANOVA – Analysis of Variance
ARAC – Aviation Rulemaking Advisory Committee
ATDs – Anthropomorphic Test Devices
ASTM – American Society of Testing and Materials
CAD - Computer Aided Design
CBR – California Bearing Ratio
CFC – Channel Filter Class
CFR – Code of Federal Regulations
CG – Center of Gravity
CID – Controlled Impact Demonstration
CNRB - Constrained Nodal Rigid Body.
DAS – Data Acquisition System
DCP – Dynamic Cone Penetrometer
FAA – Federal Aviation Administration
FEM – Finite Element Model
FS – Fuselage Station
ft – unit of length, foot or feet
g – unit of acceleration relative to the acceleration of gravity
GUS – Gantry Unwashed Sand
Hz – unit of frequency, Hertz
in – unit of length, inch
in/s – unit of velocity, inches/second
LandIR – Landing and Impact Research facility
lb – unit of force or weight, pound
LSTC - Livermore Software Technology Corporation
MPC - Magnitude-Phase-Comprehensive metric
MPP – Massively Parallel Processing
NASA – National Aeronautics and Space Administration
NASTRAN - NAsa STRuctural ANalysis code
NCAC - National Crash Analysis Center
RSVVP - Roadside Safety Verification and Validation Program
s – unit of time, second
SAE – Society of Automotive Engineering
SGC – Sprague and Geers Comprehensive
SGM – Sprague and Geers Magnitude
SGP – Sprague and Geers Phase
SMP - Symmetric Multi-Processing
SPC – Single Point Constraint
TSR – Transient Shock Recorders

Finite Element Simulations of Two Vertical Drop Tests of F-28 Fuselage Sections

by

Karen E. Jackson, Justin D. Littell, Martin S. Annett, and Ian M. Haskin

I. ABSTRACT

In March 2017, a vertical drop test of a forward fuselage section of a Fokker F-28 MK4000 aircraft was conducted as part of a joint NASA/FAA project to investigate the performance of transport aircraft under realistic crash conditions. In June 2017, a vertical drop test was conducted of a wing-box fuselage section of the same aircraft. Both sections were configured with two rows of aircraft seats, in a triple-double configuration. A total of ten Anthropomorphic Test Devices (ATDs) were secured in seats using standard lap belt restraints. The forward fuselage section was also configured with luggage in the cargo hold. Both sections were outfitted with two hat racks, each with added ballast mass. The drop tests were performed at the Landing and Impact Research facility located at NASA Langley Research Center in Hampton, Virginia. The measured impact velocity for the forward fuselage section was 346.8-in/s onto soil. The wing-box section was dropped with a downward facing pitch angle onto a sloping soil surface in order to create an induced forward acceleration in the airframe. The vertical impact velocity of the wing-box section was 349.2-in/s. A second objective of this project was to assess the capabilities of finite element simulations to predict the test responses. Finite element models of both fuselage sections were developed for execution in LS-DYNA®, a commercial explicit nonlinear transient dynamic code. The models contained accurate representations of the airframe structure, the hat racks and hat rack masses, the floor and seat tracks, the luggage in the cargo hold for the forward section, and the detailed under-floor structure in the wing-box section. Initially, concentrated masses were used to represent the inertial properties of the seats, restraints, and ATD occupants. However, later simulations were performed that included finite element representations of the seats, restraints, and ATD occupants. These models were developed to more accurately replicate the seat loading of the floor and to enable prediction of occupant impact responses. Models were executed to generate analytical predictions of airframe responses, which were compared with test data to validate the model. Comparisons of predicted and experimental structural deformation and failures were made. Finally, predicted and experimental soil deformation and crater depths were also compared for both drop test configurations.

II. INTRODUCTION

Recently, the crashworthy behavior of transport aircraft has become a topic of significant interest by the Federal Aviation Administration (FAA) and the National Aeronautics and Space Administration (NASA). In 2015, the FAA created an Aviation Rulemaking Advisory Committee

(ARAC) whose goal is to generate recommendations for establishing whole airframe crashworthiness and ditching requirements for transport aircraft [1]. To support this effort, NASA and the FAA signed an interagency research agreement in 2016 which enabled vertical drop tests of two fuselage sections of a Fokker F-28 Fellowship aircraft. The drop tests were conducted at the Landing and Impact Research facility (LandIR) at NASA Langley Research Center [2]. The portions of the airframe from which the sections were taken are highlighted in the schematic drawing shown in Figure 1.

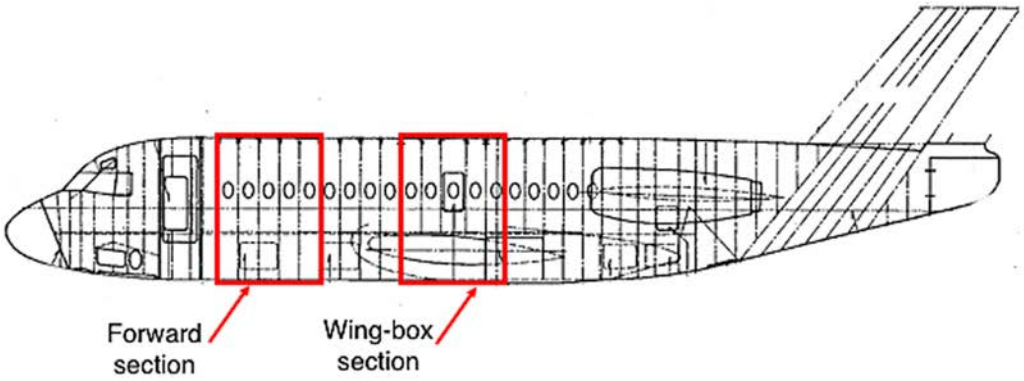

Figure 1. Side-view schematic of the F-28 highlighting the locations of the two fuselage sections.

The Fokker F-28 Fellowship is a short range jet airliner, sometimes referred to as a regional jet, that is designed and built by the Dutch aircraft manufacturer Fokker. It was originally intended to haul 50 passengers over approximately 1,000 miles, but was later reconfigured to hold 60-65 passengers. The majority of the F-28 fleet has retired from service, with only a handful of airworthy aircraft operated by African commercial carriers.

In the late 1990's, NASA Langley obtained one complete F-28 aircraft, which had been retired from service, plus three fuselage sections, for testing under the Systems Approach to Crashworthiness Program [3]. In 2001, a vertical drop test of the first F-28 fuselage section was performed [4, 5]. This section was tested at an impact velocity of 362.4-in/s onto concrete and was loaded with twenty 75-lb lead masses, attached to the seat rails, ten per side. The section was not loaded with luggage in the cargo hold and, consequently, exhibited discrete failures at the bottom centerline and at two symmetric locations on either side of the bottom centerline. The floor also buckled and failed along its centerline. Pre- and post-test photographs of this first F-28 fuselage section drop test are shown in Figure 2.

Vertical drop tests of partial fuselage sections (commonly called "barrel drops" or "barrel sections") have occurred for transport category aircraft at different times in the past. Drop tests were conducted in the 1980's at NASA Langley Research Center for the acquisition of airframe, occupant, and seat data from Boeing 707 fuselage sections [6, 7] in preparation for a full-scale crash test, known as the Controlled Impact Demonstration (CID) which occurred in 1984. More recently, drop tests of both Boeing 737 [8] and Boeing 707 [9] fuselage sections were conducted

by the FAA. A subset of these tests was used to evaluate airframe interaction with auxiliary fuel tanks present and to collect airframe, seat and occupant loads for evaluation of injury metrics. The FAA used this information as a precursor for vertical drop tests of full-scale aircraft, including an ATR42-300 [10], Metro III [11], Beechcraft 1900C [12], and a Shorts 3-30 [13]. These drop tests were conducted to investigate airframe structural responses and occupant injuries for aircraft crashes under severe but survivable conditions.

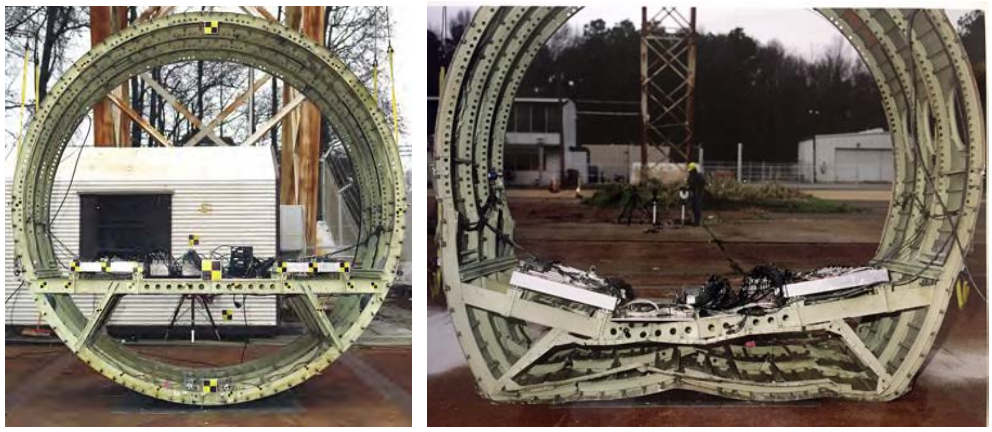

(a)Pre-test photograph. (b)Post-test photograph.

Figure 2. Pre- and post-test photographs of the 2001 vertical drop test of an F-28 fuselage section.

A second objective of the NASA/FAA collaborative effort was to assess the capabilities of analytical methods to predict the test responses. Finite element models were developed of the F-28 fuselage sections for execution in LS-DYNA® [14-16], which is a commercial code for simulating explicit nonlinear transient dynamic problems. The models contained accurate representations of the airframe structure, the hat racks and hat rack masses, the floor and seat tracks, the luggage in the cargo hold of the forward section, and the detailed under-floor structure in the wing-box section. Initially, concentrated masses were used to represent the inertial properties of the seats, restraints, and the Anthropomorphic Test Devices (ATDs) occupants. However, later simulations were performed that included finite element representations of the seats, restraints, and ATD occupants. These models were developed to more accurately replicate the seat loading of the floor and to enable prediction of occupant impact responses.

This paper will document the test set-up, model development, and test-analysis comparisons of time-history responses and structural deformations for drop tests of two F-28 fuselage sections.

III. TEST DESCRIPTIONS

This section of the paper will describe drop tests of both the forward and wing-box sections of the F-28 aircraft and will document the test set-up and experimental approach. Additional information on the experimental program can be found in Reference 17.

A. Forward Section Drop Test

In March 2017, a vertical drop test of a 10-ft-long forward section of a Fokker F-28 Fellowship aircraft was conducted onto soil at the LandIR facility located at NASA Langley Research Center. A photograph of the unloaded fuselage section is shown in Figure 3. This photograph shows the fuselage section without seats, dummies, hat racks, luggage, interior paneling, and floor panels. A pre-test photograph of the fully loaded fuselage section is depicted in Figure 4(a). Prior to the drop test, the section was configured with two rows of aircraft seats, in a triple-double configuration, as depicted schematically in Figure 4(b). A total of ten ATDs were secured in the seats using standard lap belt restraints. The section was also configured with packed luggage in the cargo hold and two hat racks, each with mass loading of 25-lb per linear foot. The planned impact velocity was 360-in/s onto a 2-ft-high soil bed.

Figure 3. Photograph of the unloaded F-28 forward fuselage section.

The forward barrel section consists of five windows and six frames between Fuselage Station (FS) 5305 and FS 7805. The interior paneling and the floor panels were removed. A cargo door is located on the lower right side of the section. The barrel section is approximately 9-ft wide at the floor. Packed luggage (922-lb) was loaded into the cargo hold of the section and was restrained by netting on both the forward and aft ends. Hat racks were fabricated by attaching c-channel beams to the upper fuselage and adding ballast weight of 116-lb per side. Floor panels were installed and cut to fit the section length, as needed. The floor was ballasted using a combination of seated ATDs and Data Acquisition Systems (DAS) to achieve a total pre-test weight of 4,465-lb. The fully-loaded fuselage section is depicted in Figure 4(a).

The vertical drop test of the F-28 forward section was performed by raising the test article approximately 14-ft in the air and releasing it to impact a 2-ft-high soil bed. The measured impact velocity was 346.8-in/s. Prior to the test, one side of the fuselage section was painted white and 1.0-in.-diameter black dots were painted on the white surface in a random pattern. The painted

dots were used as targets, which were tracked using three-dimensional full-field photogrammetry [18-20].

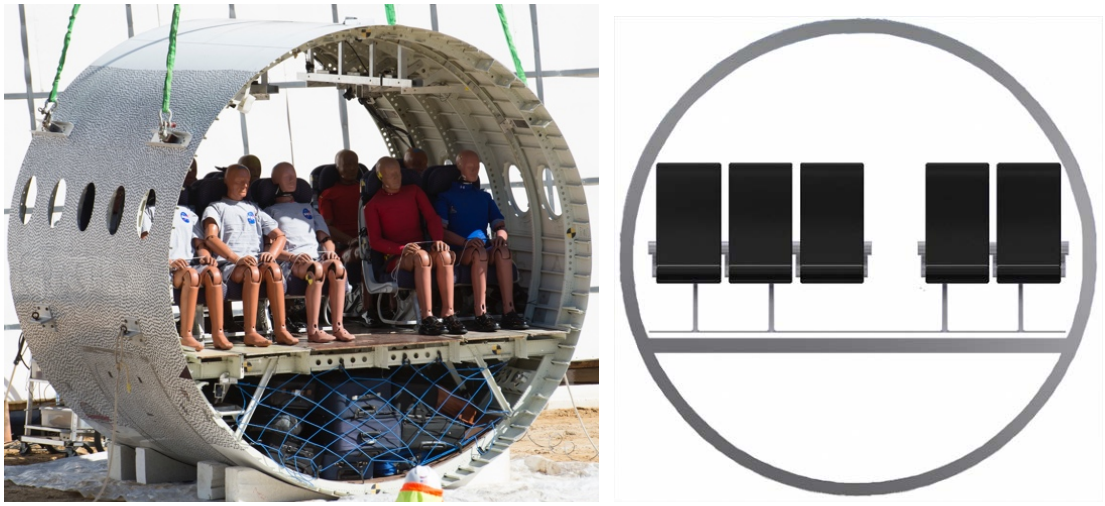

(a)Pre-test photo of the test article. (b)The 3+2 seat arrangement.

Figure 4. Photograph of the F-28 section and schematic of the 3+2 seat configuration.

The F-28 fuselage section was instrumented to collect a total of 145 channels of data at 10,000 samples per second per channel. The majority of the instrumentation was used in the collection of ATD responses. Approximately 35 channels were located on the airframe structure. Some of these channel positions are shown in Figure 5. Since the test/analysis comparisons are focused on structural responses, the seat track channels are highlighted in the test/analysis comparisons.

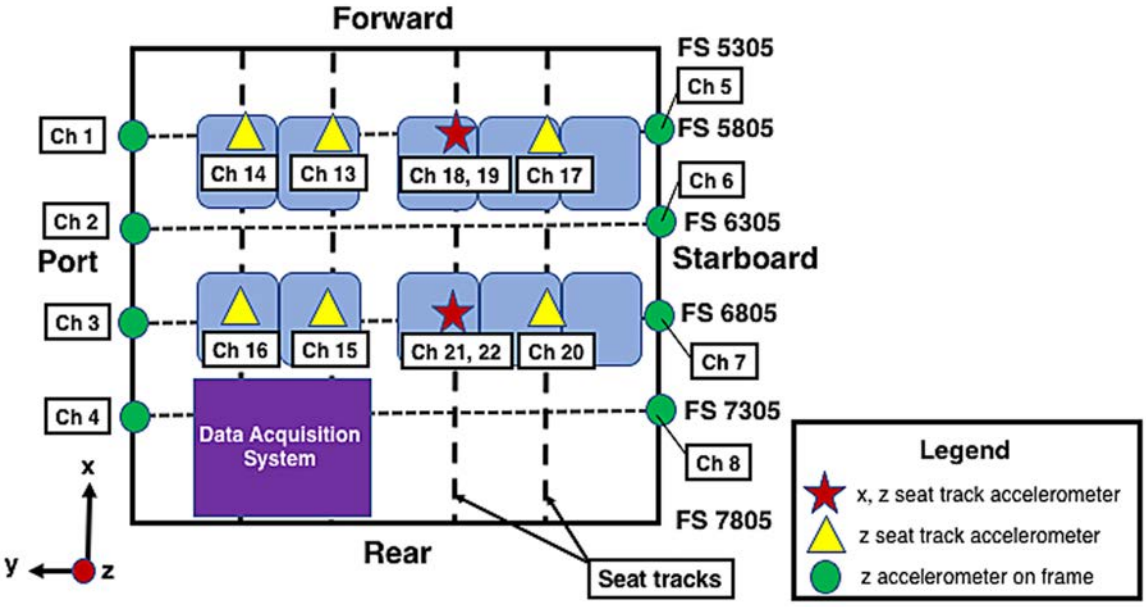

Figure 5. Instrumentation layout on the F-28 floor of the forward section.

B. Wing-Box Section Drop Test

The F-28 wing-box section was cut between FS 9805 and 12405 from a F-28 MK4000 full-scale fuselage. Figure 1 shows a schematic of a F-28 fuselage with the wing-box section highlighted. Note that the schematic shows the F-28 MK1000 variant, which is slightly smaller than the MK4000. The major difference between these two airframes is that the schematic shows only a single emergency exit, whereas the test article (the MK4000 variant) contains two emergency exits. However, the location of the test article is identical.

All of the interior structure including electronics, lighting, paneling and hat racks were removed such that only the outer skin, frames and other structural components of the airframe remained, as shown in Figure 6(a). The floors and seats were removed for storage, and while the original floors were reinstalled for the test, the original seats were discarded. The wings were removed at the wing-box attachment points, and all fluids were drained from the remaining hydraulic lines that were still present in the wing truss structure and lower cavity below the wing truss structure.

Two rows of seats were installed in a triple-double configuration, with the triple seats installed on the starboard side of the section and the double seats installed on the port side. Seats were certified to Code of Federal Regulations (CFR) Part 25.562 and they were removed from an in-service Boeing 737 aircraft. Seat legs were reconfigured to interface with the seat track dimensions of the F-28. For the seats on the double side, the window seat was cut out of a triple configuration to achieve a double configuration. Seat track accelerations were measured by attaching an accelerometer at the base of the seat leg. The rear row of seats was placed between FS 10790 and 11405 while the front seats were centered over FS 10305. The seat pitch was 32-in. between rows. All seats were placed in their most upright position and all armrests were placed up, so as not to interfere with the ATD motion. A combination of ATD sizes, ranging between 5th and 95th percentiles, were installed in the 10 seats onboard the test article. The fully loaded F-28 wing-box fuselage section is depicted in Figure 6(b).

Hat racks were created by adding lead ballast to aluminum c-channel sections, for a total weight of 232-lb (116-lb per side). Aluminum c-channels were attached to the existing locations of overhead bin attachment points on the frames and spanned between FS 10305 and FS 11905. Accelerations were measured at the hat rack-frame attachment points at FS 10305 and 11405 and on the most forward and most aft lead ballast on each side. Figure 7 shows a close-up photograph of a hat rack as installed in the airframe.

Instrumentation on the airframe included several accelerometers mounted at critical locations. Accelerometers were located on the floor/frame section junctions, seat tracks, lead ballast on the hat racks, ballast/frame attachment points for the hat racks, and under the wing-box truss structure, near the lower cavity at the bottom of the test article. Two rotational rate sensors, one in the front

and one in the rear, were added to measure the pitch rotation of the test article. Additionally, two standalone acceleration data loggers known as Transient Shock Recorders (TSRs) were added at two positions in the rear of the test article. The first was placed on a plate mounted on the outer seat track near the rear starboard side of the test article, and the second was placed on an unsupported span in the lower rear starboard cavity, near the bottom skin. These data recorders were set to initiate data logging via sensing a g-threshold limit, set at 20 g, and would record accelerations in three axes at 10 kHz for 10 seconds once initiated. An additional 6000-g shock recorder was also placed next to the TSR on the rear starboard outer seat track; however, this recorder did not trigger, and data was not collected. As an alternative, conventional accelerometers were added to the rear starboard outer seat track TSR plate to confirm the data collected by the TSR. The floor-level instrumentation layout is depicted in Figure 8 including channels located at the seat track/seat interface, the floor/frame interface, and the data systems for the wing-box section drop test.

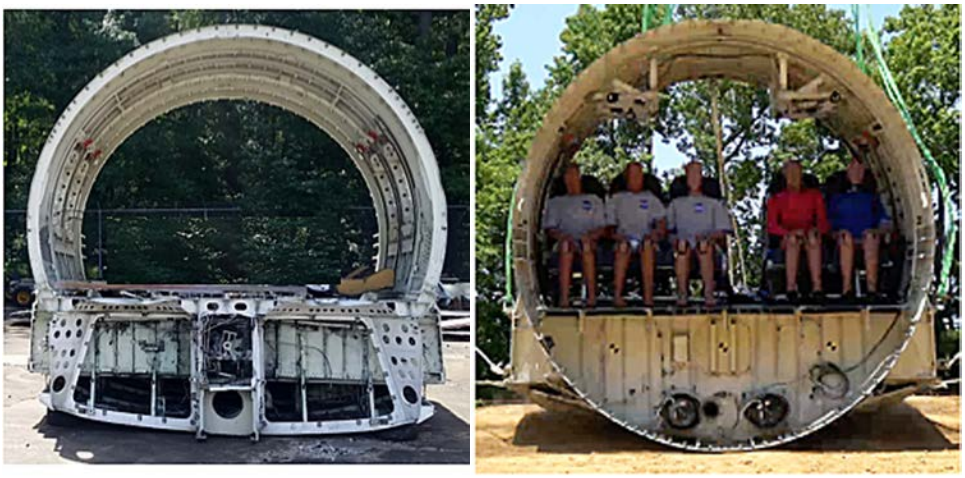

(a)Unloaded F-28 fuselage section. (b)Fully loaded f-28 wing-box section.

Figure 6. F-28 wing-box section photographs.

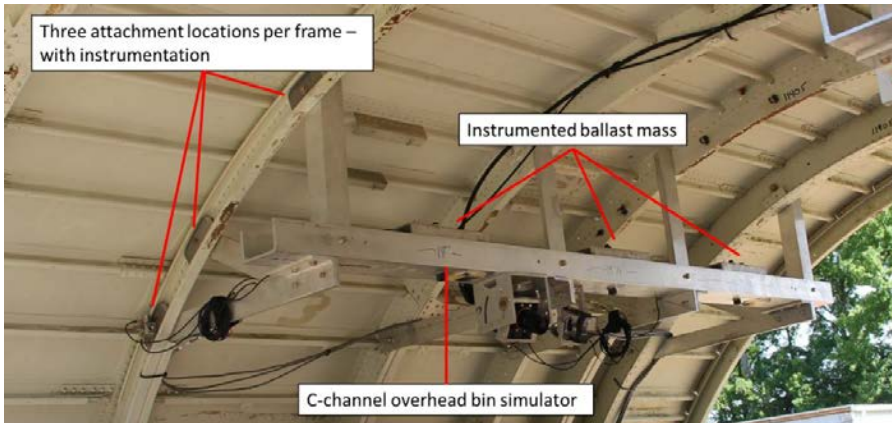

Figure 7. Hat rack simulators with ballast.

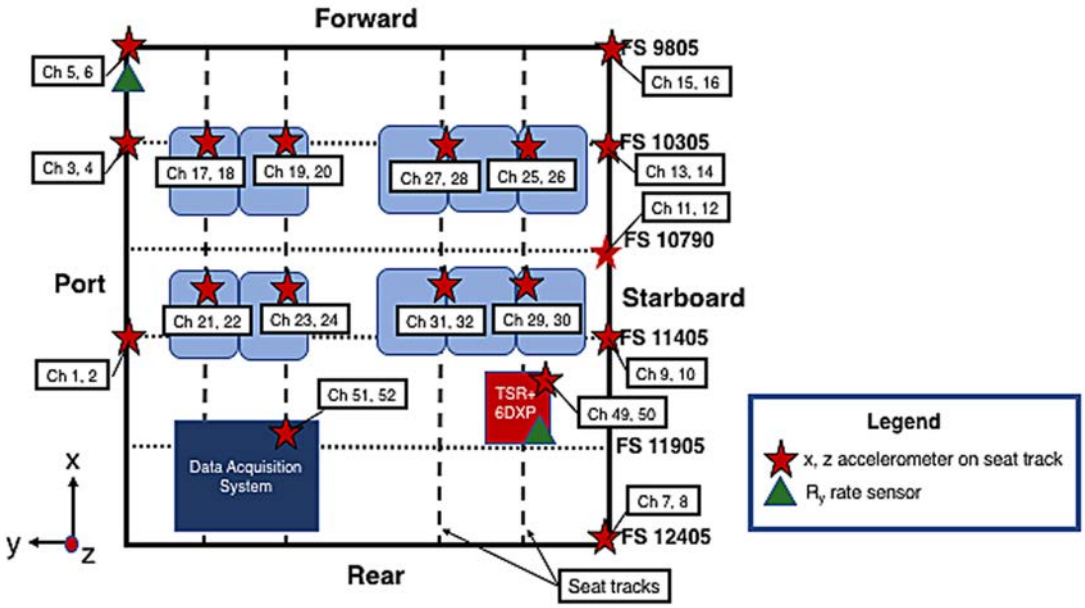

Figure 8. Floor-level instrumentation of the wing-box fuselage section.

In addition to eight onboard cameras, eight external high speed cameras were used to capture the drop from all four sides at 1000 frames per second. These cameras focused on the onboard occupant responses and general test article motion during impact. A monochromatic stochastic pattern was applied to the starboard side of the test article, in which 1-in.-diameter black dots were hand painted on one side of the fuselage section, which had previously been painted white. Each dot was used for full-field digital image correlation to determine test article deformation during the impact event [20]. Additional cameras were placed around the perimeter of the test area.

After all of the ballast, instrumentation, cameras and ATDs were installed, the total weight of the test article was 5,180 lb. The center of gravity (CG) was 4.25-in. forward of FS 10790 in the longitudinal direction and 1.4-in. starboard of the geometric center in the lateral direction. The CG vertical height was not measured. The test article was lifted to its release height using soft straps attached to swivel hoist rings that were located at the original wing attachment locations. The fuselage section was pitched downward by utilizing lower wing attachment holes for the rear lifting locations than in the front. The nominal pitch was calculated to be approximately 4.6°; however, the pitch angle at impact was 2.9°. The measured impact velocity was 349.2-in/s.

The test article impacted a mound of soil that was placed over the concrete pad located beneath the LandIR facility. Soil, that was designated Gantry Unwashed Sand (GUS) [21] was built into a 20-ft by 20-ft square mound, with a downward facing 10° slope, such that the rear portion of the test article would contact first, causing a rotational velocity component about the rear impact point. This rotation would cause the forward portion of the test article to impact at a downward pitch angle. The rotation was designed to induce a forward acceleration into the onboard ATDs. The properties of the soil were measured on test day, approximately 1 hour before the test occurred.

C. Soil Characterization Testing

Since both F-28 fuselage sections were dropped onto soil, it is important to document the soil characterization procedures. A variety of factors contribute to the variability of soils, especially for dynamic impacts. The microstructure of the soil, the grain size of the soil, and the void between particles or grains can be very important. In addition, the same soil can behave quite differently for dynamic impacts depending on the moisture content. The pores between the grains can be filled with either highly compressible air or with water. The strength of coarse soil materials, such as gravel, depends highly upon gravitational effects, and the materials essentially have no inherent constitutive law. For small-particle soils, such as clays, constitutive equations do apply, and cohesion can be important. In contrast, sand has no tensile strength when dry, but wet sand does have some tensile strength due to cohesion. Note that the GUS soil used for the fuselage section drop tests was a mixture of sand and clay [22].

All of the soil characterization tests were performed on test day either before or after the impact occurred. For both drop tests, three locations were selected for soil characterization testing. Three different soil characterization tests were performed: Ball penetrometer tests, Dynamic Cone Penetrometer (DCP) tests, and soil sample tests. Each of these tests will be described, as follows.

The ball penetrometer is comprised of a hollow steel hemisphere weighted with lead and a plate for mounting a TSR shock recorder. The device is released from a height of 29-in. above the soil surface using a drop height indicator for consistency. For each event, the depth and diameter of the resulting crater in the soil are measured and recorded. The ball penetrometer has a diameter of 8-in., and a weight of 18.7-lb. During impact with the soil, data are recorded at 10,000 samples per second and the response is triggered at a threshold of 10-g. A photograph of the ball penetrometer is shown in Figure 9. Often, ball penetrometer tests are simulated in LS-DYNA as a means of calibrating the soil model [22].

Figure 9. Ball penetrometer with TSR shock recorder.

Measurements of the strength and relative thickness of the soil layers are obtained using a Kessler DCP. The DCP consists of a hardened steel cone at the end of a stainless-steel rod driven into the soil by blows of a 10.1-lb hammer. The DCP is shown in Figure 10. Measurements of the distance travelled by the cone are taken every 1 to 4 blows and the distance between data points can vary between 0.315- and 4.92-in. The penetration data are then used to determine an estimate of the California Bearing Ratio (CBR) and the bearing capacity [21-23]. The resulting CBR and bearing capacity data are compared to known soil descriptors, shown in Table 1.

Figure 10. Photograph and schematic of the Dynamic Cone Penetrometer.

Table 1. Soil descriptions based on bearing capacity.

Soil Description	Bearing capacity, psi
Hard soil	>22
Stiff soil	10.8-22
Firm soil	5.8-10.8
Soft soil	2.9-5.8
Very soft soil	<2.9

Three soil samples were taken around the perimeter of the test article in the area of the impact for each drop test to identify moisture content and to provide a wet and dry density of the soil on test day. As shown in Figure 11, a metal cylinder was driven 6-8 inches into the soil to generate a cylindrical slug of soil. The diameter and length of the slugs were measured and the samples were weighed to generate a wet soil density. Smaller samples of the soil, one taken from each of the three slugs at about three inches from the soil surface, were crumbled into beakers. The beakers were weighed and placed into an oven to bake at 220°-260° Fahrenheit for 22- to 24-hours. The

beakers were then re-weighed after baking. The resulting moisture content and dry soil properties of the samples are tabulated.

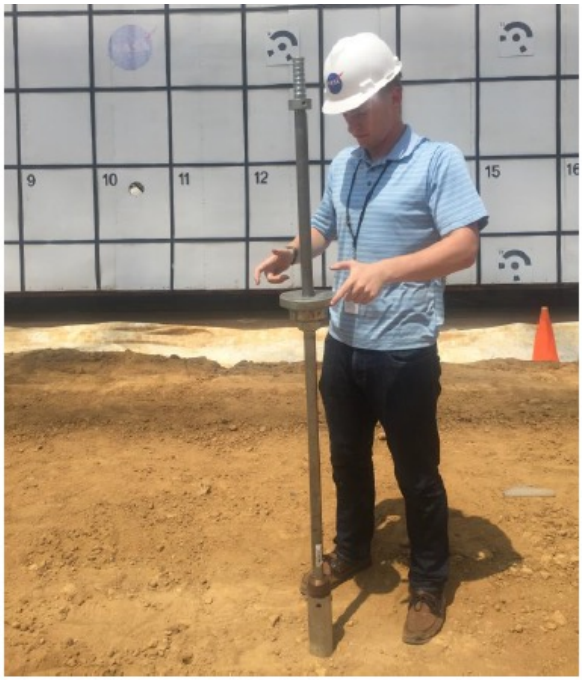

Figure 11. Soil sample tool in use.

i. F-28 Forward Fuselage Section Soil Characterization

For the F-28 forward fuselage section, the impact surface was a 15-ft wide, 20-ft long, 2-ft high soil bed. Soil characterization tests were performed after the F-28 forward fuselage section impact test and prior to removal of the test article. Ball penetrometer and drop cone penetrometer tests were performed at three locations. In addition, soil samples were taken at three locations. The measured average moisture content of the soil was 11.4%. The peak resultant accelerations and the depth and diameter of each ball penetrometer crater are summarized in Table 2. The data shown in Table 2 indicate that the soil is highly variable with peak resultant accelerations ranging from 44- to 56-g.

Table 2. Ball penetrometer data from 3 drop tests following the F-28 forward section impact.

Location	Depth (d), in	Diameter (w), in	Peak Resultant g's
1	1	6	44
2	½	4 ¼	46
3	5/8	4 ¾	56

Typical CBR and bearing capacity plots are shown in Figures 12(a) and (b), respectively, for the F-28 forward fuselage section soil, as determined from DCP tests. Comparing the values shown

in Figure 12 with the soil descriptors shown in Table 1, the soil may be categorized as a firm soil. Finally, results of the soil sampling tests are shown in Table 3.

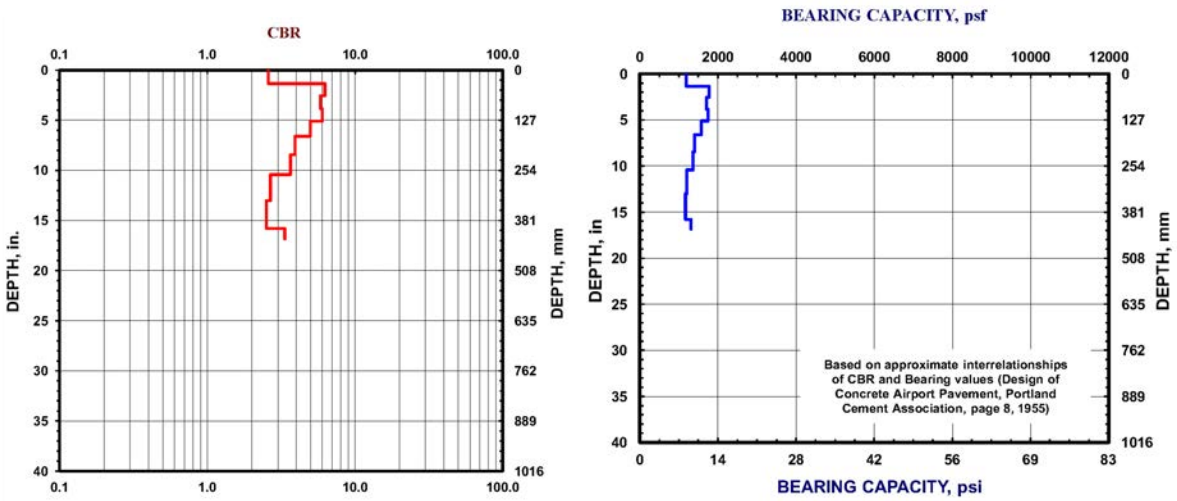

(a)CBR plot. (b) Bearing capacity plot.

Figure 12. CBR and bearing capacity data recorded following the F-28 forward section drop test.

Table 3. Soil Density and Moisture Content

Wet Soil Density	133.5 lb/ft^3	131.7 lb/ft^3	140.2 lb/ft^3
Dry Soil Density	119.5 lb/ft^3	118.0 lb/ft^3	126.7 lb/ft^3
Moisture Content	11.7 %	11.7 %	10.7 %

ii. F-28 Wing-Box Fuselage Section Soil Characterization

Soil characterization for the wing-box section was performed before the test occurred. Data were collected from three locations around the perimeter of the test article. Only a few ball penetrometer tests were conducted and, since these data were not used for model calibration, they are not reported. DCP tests were performed and sample plots of CBR and bearing capacity are shown in Figure 13. Comparing the values shown in Figure 13 with the soil descriptors shown in Table 1, the soil may be categorized as a firm soil.

Three soil samples were taken following the wing-box section test, one from the top and bottom of the inclined soil pile and one from the center of the pile/impact location. The soil samples were baked at between 240°-260° for a period of 24 hours. The average properties for the soil samples are: Moisture Content = 8.4%, Wet Density = 124.4 lb/ft^3 and Dry Density = 114.7 lb/ft^3.

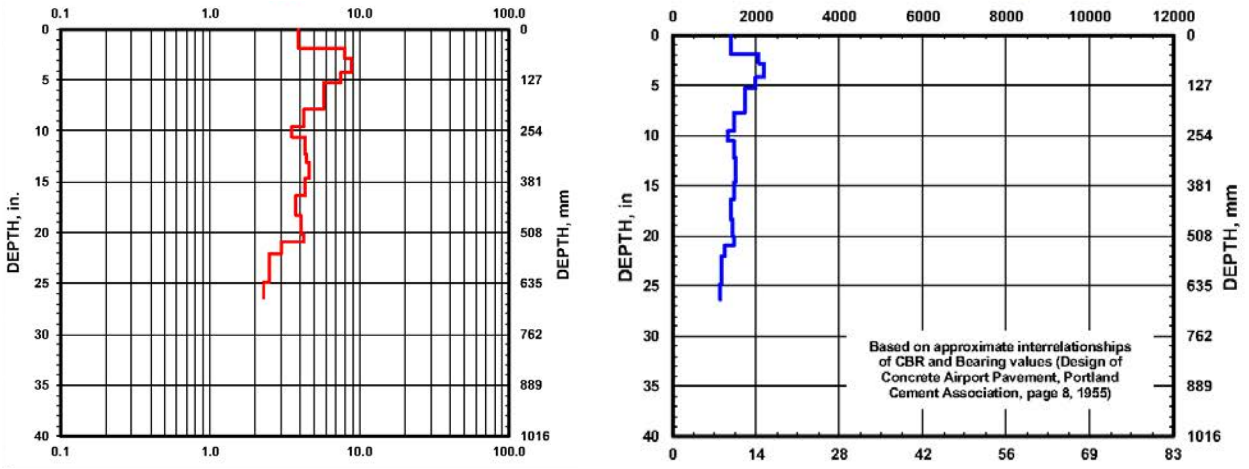

(a)CBR plot. (b) Bearing capacity plot.

Figure 13. CBR and bearing capacity data recorded following the F-28 wing-box drop test.

IV. MODEL DEVELOPMENT

This section of the paper will describe the development of finite element models used to represent both the forward and wing-box fuselage sections. Each model was executed in LS-DYNA® using Symmetric Multi-Processing (SMP) Version 971.

A. Forward Section Model

The LS-DYNA® model, shown in Figure 14, was created from a NAsa STRuctural ANalysis (NASTRAN) model of the F-28 Fellowship aircraft that was provided to NASA by Fokker at the time of original purchase of the airframe hardware. The total weight of the structural model (minus the soil) is 4,310.8-lb, which includes 922.8-lb of luggage; 2,044-lb of floor loading; 232-lb of total hat rack mass; 170-lb for the DAS box; and 942-lb for the fuselage empty weight. The measured weight of the fully loaded F-28 fuselage section is 4,465-lb. Thus, the model is approximately 154-lb too light. The model contained: 114,636 shell elements; 48,716 solid elements; 141,080 nodes; 36 parts; 10 materials; 1 contact definition; 1 initial velocity card; and, 1 Single Point Constraint (SPC) boundary condition that was used to fix the side and bottom nodes of the soil.

Most of the material models were converted directly from the NASTRAN model to represent aluminum components using an elastic-plastic material model in LS-DYNA®. The floor panels were constructed of two different materials: aluminum-clad balsa wood, or fiberglass covered Nomex® honeycomb. Since no material properties were available for the floor panels, test specimens were obtained and three-point flexure tests were conducted and simulated to obtain material properties for these parts, as shown in Figure 15. The luggage was represented using solid elements that were assigned material properties obtained from a quasi-static crush test of stacked luggage, as described in Reference 24. A material model (*MAT_SOIL_AND_FOAM)

was assigned to the soil, as reported in Reference 22. All nodes forming the bottom and side surfaces of the soil block were fixed (i.e., no translational or rotational motion allowed) using SPCs in the LS-DYNA® model.

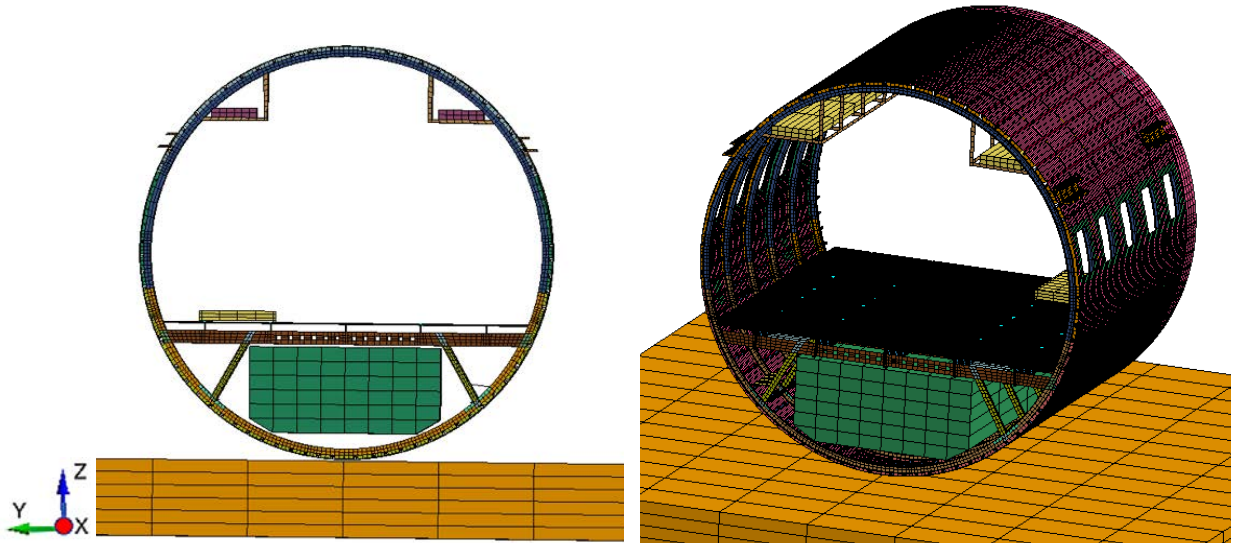

(a)Rear view of model. (b) Three-quarter front view of model.

Figure 14. Views of the finite element model of the F-28 fuselage section.

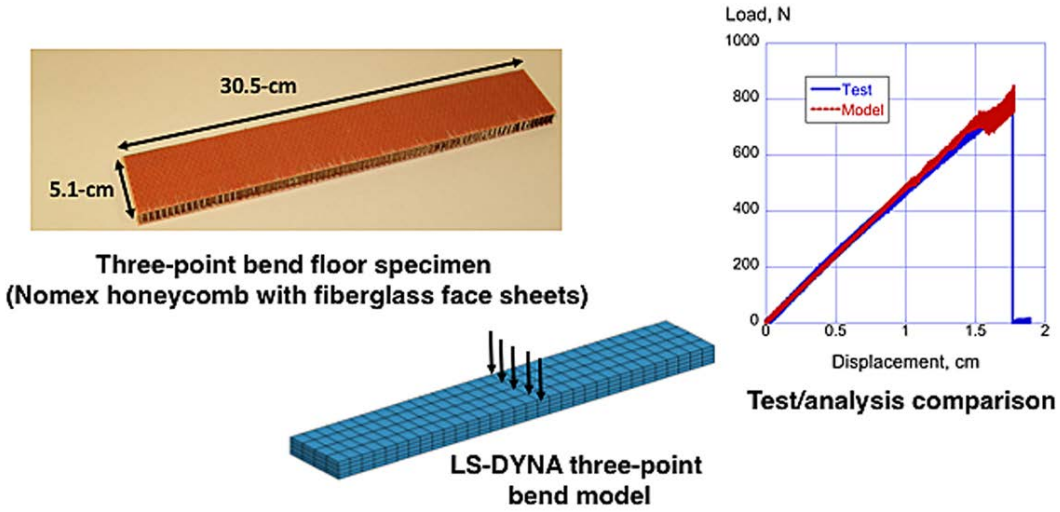

Figure 15. Three-point bend testing and simulation of floor panels.

The nodes forming the fuselage section were assigned an initial velocity of 346.8-in/s in the downward vertical direction, matching the measured velocity. An automatic contact was defined that prevents any node from penetrating any surface. For these initial simulations, the inertial properties of the seats, occupants, and restraint systems were represented using concentrated masses, placed on the floor at the approximate locations of seat attachment points. The model was executed for an end time of 0.2-s and required 35 hours of execution time running LS-DYNA SMP Version 971 double precision, on 8 processors of a workstation computer. Output requests

included time history responses corresponding to accelerometer locations and structural deformations.

B. Wing-Box Section Model

Two views of the finite element model of the F-28 wing-box section are shown in Figure 16, a side view and a three-quarter view. The model consists of 78,863 nodes; 7,566 beam elements; 16,636 shell elements; 54,436 solid elements; 794 parts; 75 material cards; 16 concentrated masses; 1 contact definition; 1 initial velocity card; and, 1 SPC boundary condition that was used to fix the side and bottom nodes of the soil. As shown in Figure 16(a), the soil is canted by 10° with respect to the global x-axis and the section is pitched down by 2.9° at impact. Due to the pitch attitude, local coordinate systems were defined at each concentrated mass on the floor. Initially, concentrated masses were used to represent the inertial properties of the seats and occupants and they were located in the model at the approximate seat attachment locations on the floor. Nodal output was requested in the local coordinate system, which moves with the model as it deforms. A close-up picture of the floor of the wing-box section is shown in Figure 17 that highlights accelerometer locations and the corresponding nodes for which output was requested in the local coordinate systems.

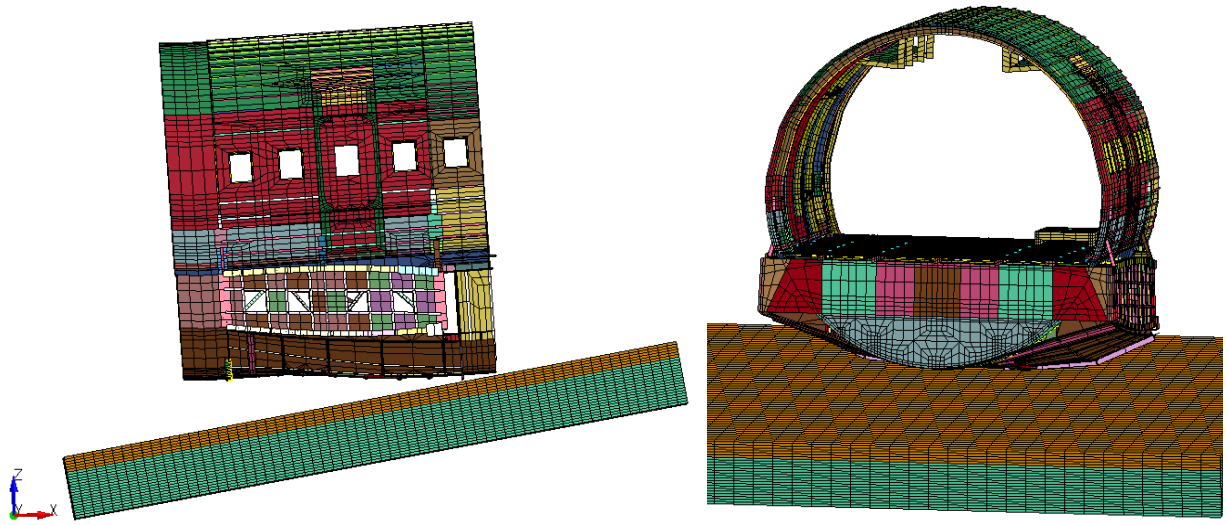

(a)Side view. (b)Three-quarter view.

Figure 16. Two views of the finite element model of the F-28 wing-box section.

One obvious difference between the forward section and the wing-box section models is that a layered soil configuration was used in the wing-box model. In this case, the top 6 soil elements through the soil depth (which represents 6-in. of soil depth out of a total of 24-in.) were assigned properties of hard soil, whereas the bottom 18 soil elements were assigned properties of soft soil. These properties were input using *MAT_SOIL_AND FOAM or Mat 5 is LS-DYNA®. The soil models have been previously reported in References 22 and 25. Another difference between the forward section and the wing-box section models is the large number of beam elements in the

wing-box model that were used to define the detailed under-floor structure. Note that the forward section model was modified such that all beam elements were replaced with shell elements. The beam elements in the wing-box model are depicted in Figure 18.

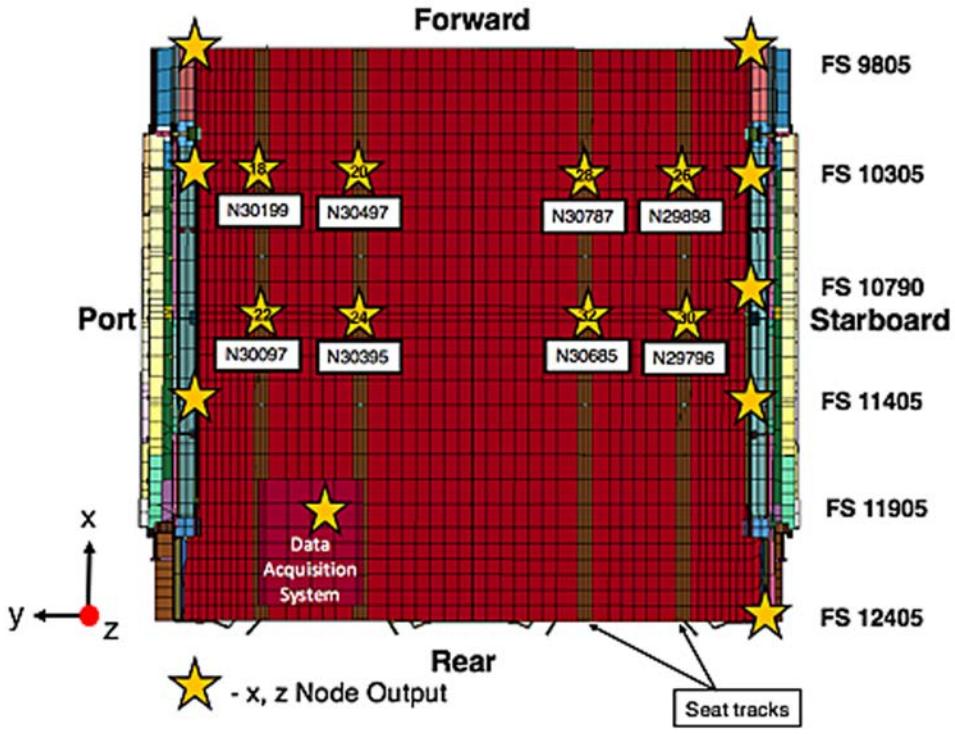

Figure 17. Depiction of the model floor layout showing test channels and nodal output locations.

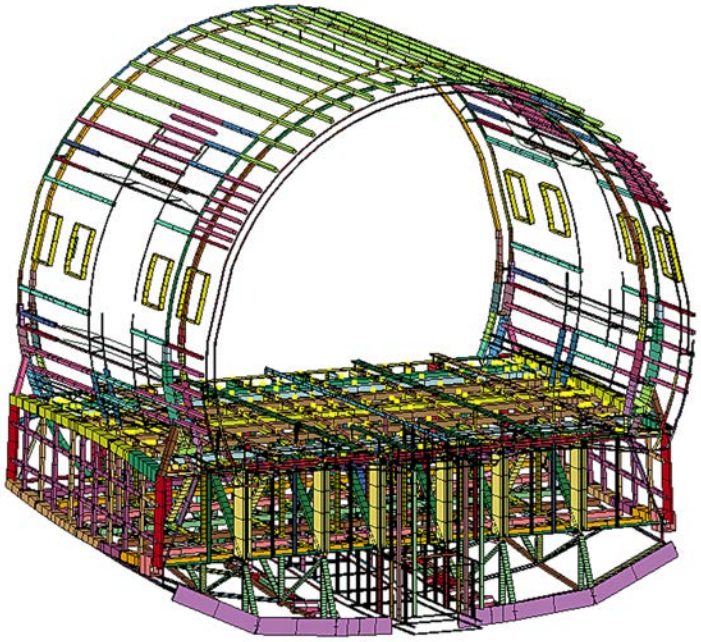

Figure 18. Beam elements in the wing-box section model.

The structural model weighed 5,127.4-lb, which is only 52.6-lb lighter than the measured weight of the test article (5,180-lb). The total weight of the model included 2,044-lb of concentrated masses on the floor representing the seats, occupants, and restraint systems; 209.4-lb for the DAS box; 232-lb for the hat rack masses; and, 2,642-lb for the empty section weight. All nodes in the wing-box section structural model were assigned an initial velocity in the global z-direction of 349.2-in/s, matching the test condition. The model was executed for an end time of 0.2-s and required 54 hours and 45 minutes of execution time running LS-DYNA® SMP Version 971 double precision, on 8 processors of a workstation computer. Output requests included time history responses corresponding to accelerometer locations and structural deformations.

C. Seat and ATD Model

While correlation efforts for the F-28 forward section model with concentrated masses were ongoing, finite element models of the seats and ATDs were developed. The plan of fully integrating the seats and ATDs with the airframe section models was contingent upon component and seat-level analyses accurately representing the occupant behavior seen in the tests. Development of the seat and ATD finite element model utilized a hierarchical approach, starting with coupon tests followed by sub-component tests.

Due to the triple-double seating configuration of the Fokker F-28, two- and three-seat finite element models were required. These models were developed through a variety of methods, including reverse engineering via electronic scans and hand measurements, as well as manipulating existing Computer Aided Design (CAD) models. Prior to model development, three-dimensional scans were taken of a full two-seat assembly, producing point clouds. These point clouds were manipulated to produce preliminary models of structural components in the seat assembly, and the models were supplemented by hand measurements. However, when converting the point cloud into a usable mesh, the model that was created had extremely low resolution. The model was comprised of many smaller components and the point density was too coarse to accurately represent individual components of the assembly. Manual digitization of components was also attempted, but resulted in skewed models.

The manufacturer of the seat, B/E Aerospace (now Rockwell Collins), then provided a CAD model of a three-seat assembly, shown in Figure 19. This model was reduced to individual part files relevant to the structural analysis, and these parts were imported into AutoDesk Inventor for geometry simplification. Solid-element models were converted to surfaces, and complex surface features irrelevant to the structure of the seats were removed. Features such as aesthetic plastic covers and cable attachment points were not included. Once component-level geometry was simplified, the CAD geometry was reassembled and exported to MSC/Patran, where the geometry model was finalized and meshed.

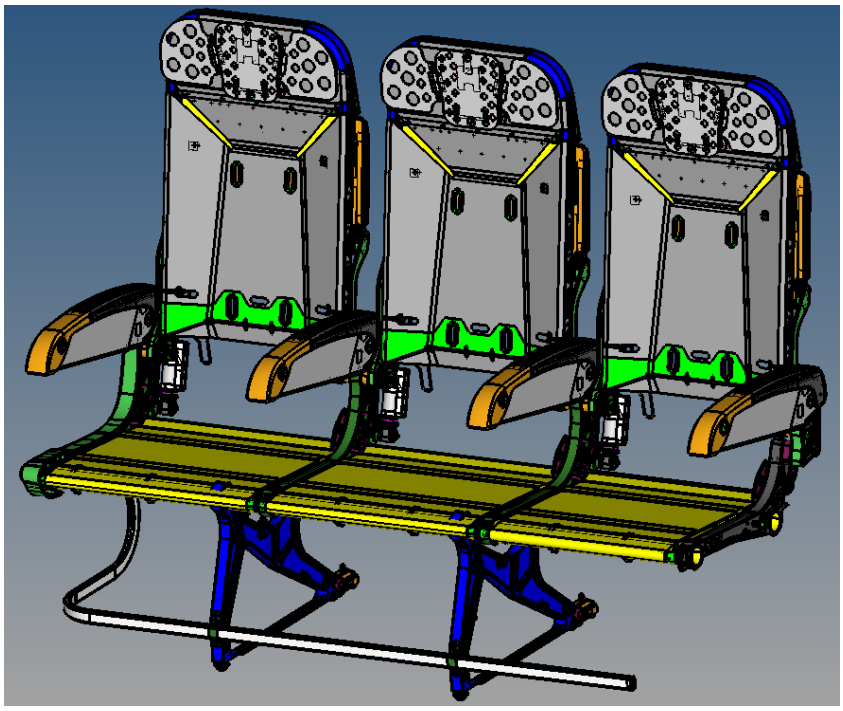

Figure 19. Seat CAD geometry model.

The seat model contains all components relevant to the structural analysis, including the legs, tubes, tube supports, seat back frame, contoured back plate, arm rests, leg rail, and seat and back cushions. The legs were laterally adjusted to align with the F-28 seat tracks. Due to the allowable clearances between the fuselage walls and the seat tracks, the aisle seat for the three-seat configuration was highly cantilevered. The overall mesh is shown in Figure 20, and mesh detail for the tube support and legs is shown in Figure 21. The element edge lengths for the structural components such as the tubes, legs, supports, and baggage bar ranged from 0.2- to 0.3-in.

The seat legs and arm supports were clamped to the seat tubes, seat back, and baggage bar with rigid attachments. Penalty contact was defined between the seat pan and the support tubes. Tied penalty contact was defined between the seat cushion and the seat pan.

The material properties of the aluminum components were assumed to be elastic-plastic and were represented in LS-DYNA using *MAT_PIECEWISE_LINEAR_PLASTICITY. The material properties are listed in Table 4. No failure strain was defined, because the metallic components were not expected to fracture, only plastically deform. The shell element formulation was ELFORM type 16, which is fully-integrated, but selectively reduced to prevent element locking.

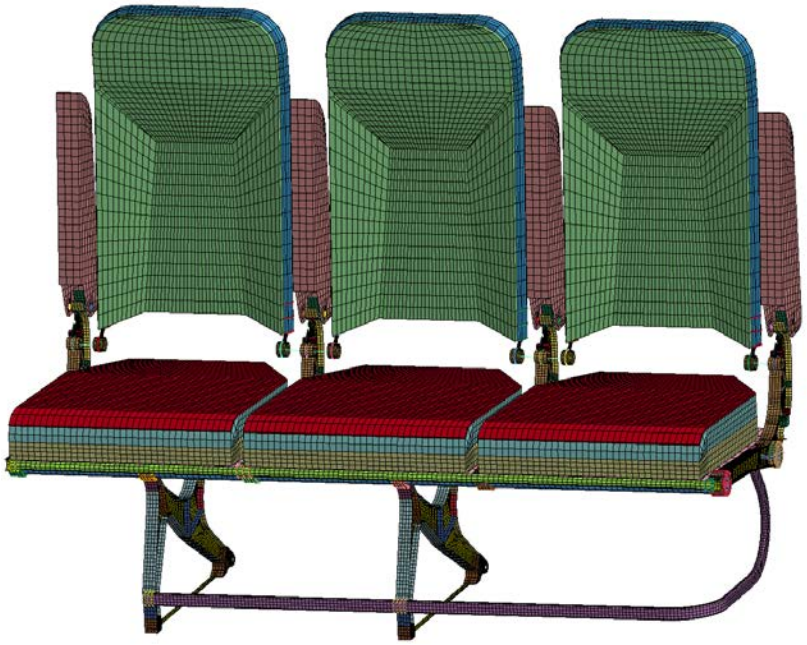

Figure 20. Seat finite element model.

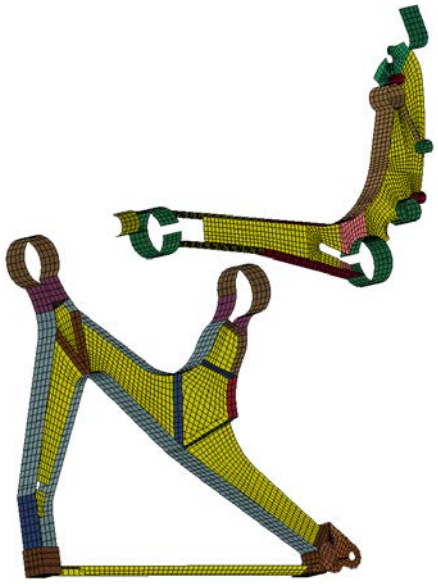

Figure 21. Leg and arm support mesh.

Table 4. Aluminum material properties.

Density	**lb/in^3**	**0.1**
Young's Modulus	psi	1e7
Poisson's Ratio		0.33
Yield Stress	psi	40,000
Tangent Modulus	psi	2e5

The stiffness properties of the seat cushion cover and the seat pan fabric were determined by tensile testing of 1-in. by 10-in. strips. A photograph of the tensile test of the seat cushion cover and a sample force-deflection plot from a test of the seat pan fabric are shown in Figure 22. Table 5 shows the *MAT_ELASTIC properties used for the seat cushion cover and the seat pan fabric.

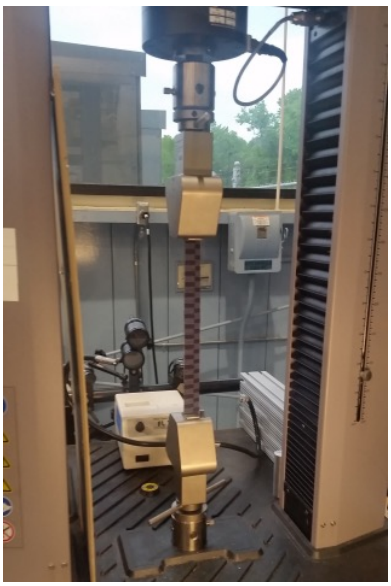

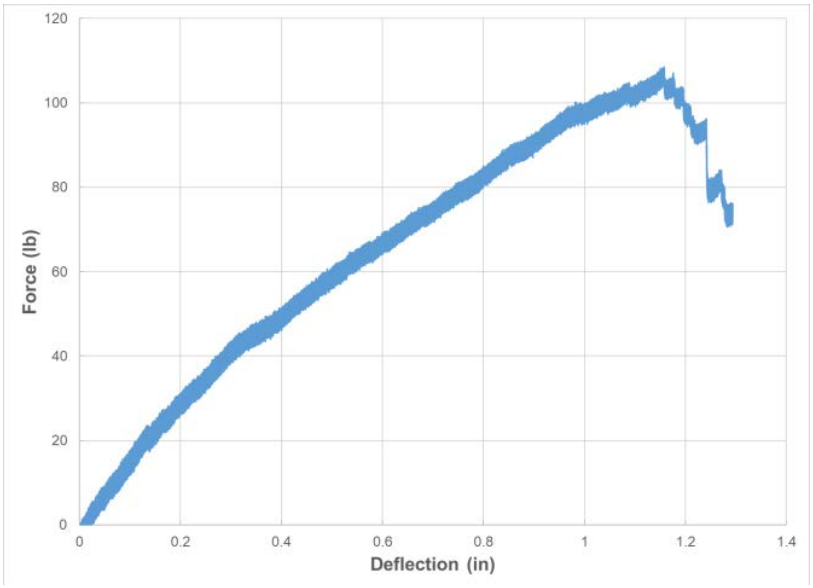

(a) Tensile test of a seat cushion cover. (b) Tensile test data of the seat pan fabric.

Figure 22. Fabric tensile tests.

Table 5. Fabric Material Properties

	Units	Seat Cushion Cover	Seat Pan Fabric
Density	lb/in^3	0.08	0.02
Young's Modulus	Psi	2,000	7,400
Poisson's Ratio		0.33	0.3

The seat cushion is composed of two different materials, an upper polyurethane layer and a lower polyethylene layer. The materials were tested by sectioning the foam into 2-in. by 2-in. by 1-in. blocks and compressed at a rate of 16-in/s. The densities of the polyurethane and polyethylene foams were calculated as 0.0018-lb/in^3 and 0.0014-lb/in^3, respectively. A photo of the foam compression test set-up and the force deflection data for the polyethylene and polyurethane are shown in Figure 23. The force/deflection data were converted to true stress versus true strain and extrapolated for higher compaction volumetric strains. The curves were included in both the *MAT_LOW_DENSITY_FOAM and *MAT_FU_CHANG material models.

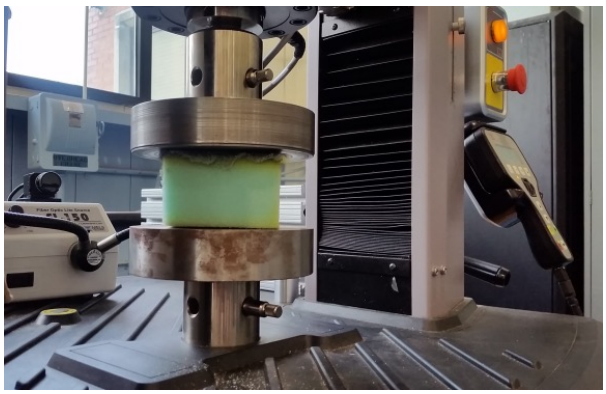

(a) Polyurethane foam compression test.

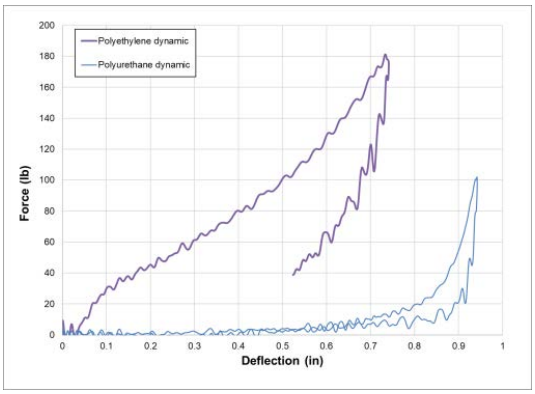

(b) Force/deflection response.

Figure 23. Foam dynamic compression tests.

Validation of the fabric and foam models was performed with drop tests of an 18-lb, 8-in.- diameter ball penetrometer onto the seat cushion. An accelerometer is mounted inside the ball penetrometer to measure the vertical deceleration. The impact velocity was 13-ft/s, and several drops were conducted. The average deceleration data is plotted versus an LS-DYNA predicted response of the test drop. The test setup, LS-DYNA simulation, and the test-analysis average vertical deceleration plot are shown in Figure 24. Both pulse durations were well matched at approximately 0.030-s. The average peak acceleration of the test was 55-g, while the peak model response was 45-g, which is an 18% difference. It was evident that the predicted response is highly sensitive to several parameters: (1) material model selection (*MAT_LOW_DENSITY_FOAM versus *MAT_FU_CHANG_FOAM), (2) foam material coefficients to prevent hourglassing, (3) scaling of the foam stress/strain curve, and (4) viscous damping coefficients. Ultimately, *MAT_LOW_DENSITY_FOAM was selected and the model parameters were calibrated to best match the penetrometer drop test results.

Test Setup

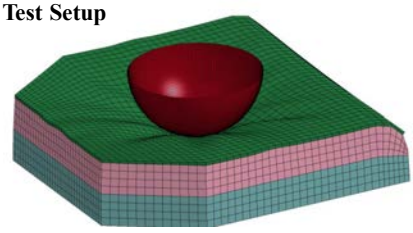

LS-DYNA Simulation

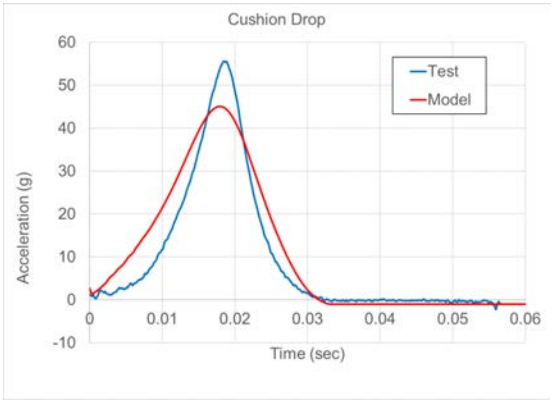

Figure 24. Seat cushion drop test and model calibration.

With increased confidence in the seat model development, the next step was to integrate finite element models of the ATDs. The two 50th percentile ATDs that were used in the F-28 section drops were either a Hybrid II or an FAA Hybrid III, both containing straight lumbar spines. These two ATDs are specified for use in aircraft seat certification sled tests, during which the dummy is seated in a more upright position relative to the slouched posture of the automotive Hybrid III. The software developer of LS-DYNA, Livermore Software Technology Corporation (LSTC), makes available a 50th percentile automotive Hybrid III model for LS-DYNA users. The model was originally developed jointly with the George Washington University National Crash Analysis Center (NCAC) and is known as the "LSTC Detailed Finite Element Model (FEM)." The LSTC Detailed FEM [26] has been calibrated for automotive frontal impact conditions, with emphasis on capturing head/neck and chest kinematics. The LSTC Detailed FEM has only recently been used in simulations that involve predominantly vertical loading, as seen in the F-28 section drops. This dummy model also includes the automotive curved spine, with the lumbar load cell angled at 22° compared to the straight spine. Nevertheless, the weight of the LSTC Detailed FEM is within 5-lb of the Hybrid II and FAA Hybrid III ATDs and is well-conditioned to represent the head and torso flail kinematics of the ATD as it sinks into the seat cushion and deforms the seat. Vertical pelvic accelerations could therefore be compared between test and analysis to assess model adequacy.

Because the LSTC Detailed FEM contains over 450,000 elements, it was not practical from a runtime standpoint to include the dummy model in all seats. Two seats were chosen, both on the aisle, to include the detailed occupant models. These two locations bound the response of the ATDs. The triple aisle seat showed the minimum lumbar loads due to the aft seat tubes bending and permanently deforming. The double aisle seat was located directly above a seat leg, and showed the highest lumbar loads. For the remaining seats, a rigid torso and pelvis mass surrogate was included that weighed 150-lb and was intended to load the seat cushion similarly to the detailed occupant models. All ATD models and mass surrogates were restrained with lap belts. The positioning of the LSTC Detailed FEM models was based on overlays of laser scan point clouds of the pre-test configurations. A LSTC Detailed FEM and rigid mass surrogate are shown in a double seat configuration in Figure 25.

An acceleration time history was applied at the base of the double and triple seat using *BOUNDARY_PRESCRIBED_MOTION. The acceleration was taken from an accelerometer located at the seat/floor interface, and has a trapezoidal pulse with an average acceleration of 10-g over 0.1-seconds. The motion of the ATDs at the time of peak deformation of the seat cushion is shown in Figure 26. Large cross tube deformation is visible in the triple seat. The applied acceleration response is plotted along with the test and analysis pelvic accelerations for the double and triple seated ATDs in Figure 27. The acceleration responses are low-pass filtered according to Society of Automotive Engineering (SAE) Channel Filter Class (CFC) 1000 [27]. The analysis shows a negative spike at the beginning of cushion compression in both the triple and double seats,

indicating spurious motion in the pelvic section as it is initially loaded. In the double seat, there are loading and unloading phases within the overall pulse that also indicate shifting in the ATD pelvis, which is not seen in test.

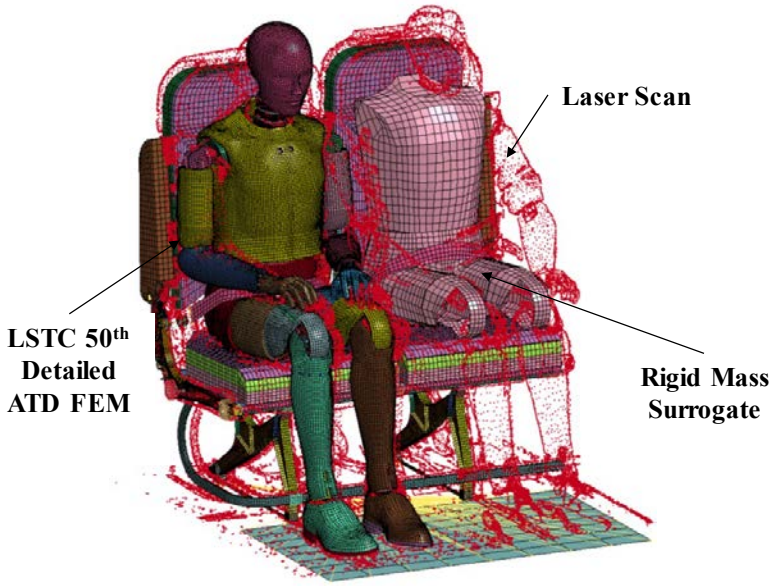

Figure 25. Combined LSTC Detailed FEM, rigid torso model, and double seat model with laser scan overlay.

For the triple seat, the test-analysis acceleration responses exhibit peaks at 20-g with a pulse duration of 0.12-s. The rise time of the analytical response is shorter than the test response, indicating that the foam may be too stiff or that foam compaction is reached too soon. For the double seat, the test-analysis acceleration responses exhibit peaks of 30-g with a pulse duration of 0.090-s. Overall, the comparison of the duration and magnitude of the responses is reasonable, but the pulse shapes are not in agreement.

Figure 26. Deformation of a single row of seats with two LSTC Detailed FEM occupant models and three rigid torso models.

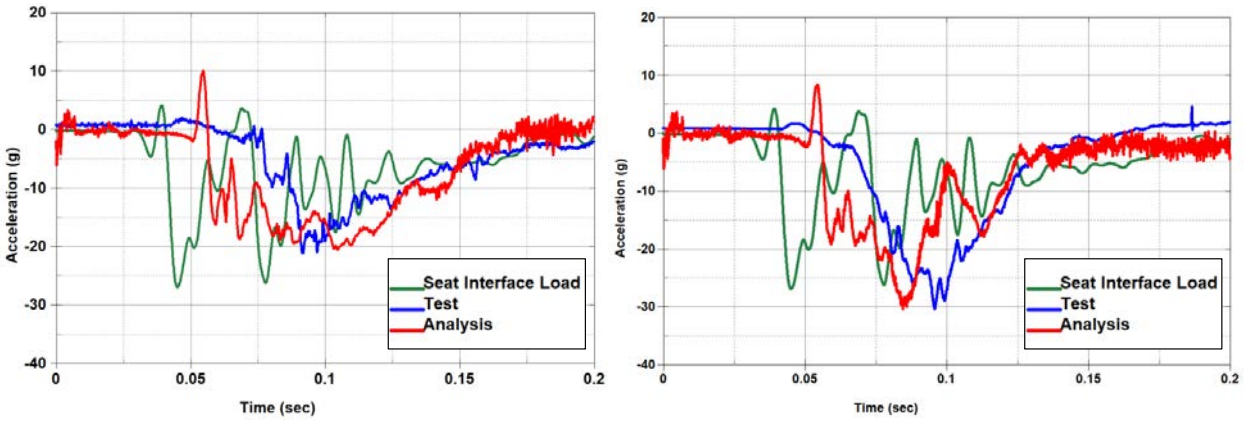

(a)Pelvic z-accel. of the triple seat ATD. (b) Pelvic z-accel. for the double seat ATD.

Figure 27. Pelvic z-acceleration response – LSTC Detailed FEM model of the ATD and seat.

V. TEST-ANALYSIS COMPARISONS

The vertical acceleration and velocity time history responses of the test data are compared with the analytical predictions for the F-28 forward section. In addition, airframe deformations and failures are compared in this section of the paper. Essentially, the time history comparisons are shown in two parts. Initially, the acceleration comparisons are presented for the simulations of the F-28 section drop tests in which the inertial properties of the seats, dummies, and restraint systems were represented using concentrated masses. Later, time history comparisons are included for simulations in which the seats, restraints, and dummies are modeled using finite elements. In addition, soil deformation data are compared. For the F-28 wing-box section, test-analysis comparisons are made initially for vertical and forward acceleration responses, based on simulations in which the seats, restraints, and ATD occupants were represented using concentrated masses. Airframe deformations and structural failures are compared, as well as soil crater depths. Final simulations were executed in which physical representations of seats, restraints, and ATD occupants were modeled.

A. F-28 Forward Fuselage Section

i. Acceleration and Velocity Time Histories

Test data were reduced following the drop test, according to the procedures outlined in Reference 28 and this analysis indicated that several channels were over-ranged, including Channels 18 and 19 (see Figure 5). Consequently, test/analysis comparisons for these channels are not shown. Please note that the experimental and analytical acceleration responses were both filtered using a

SAE CFC 60 low-pass filter [27]. Also note that test velocities were obtained by integration of the raw acceleration data. For the model, velocity data were output directly from the simulation.

The test/analysis comparisons of vertical acceleration and velocity responses are shown in Figures 28(a) and (b), respectively, for the port window location at FS 5805 (see Figure 5). At this location, the model exhibits four acceleration peaks, the first two peaks are higher in magnitude than the test. However, the overall pulse durations are similar. It is also interesting to note that, even after filtering using an SAE CFC 60 filter, the test signal contains more high frequency content than the analysis. This finding is likely due to the damping effect of adding concentrated masses in the model. The velocity responses at this location, shown in Figure 28(b), indicate that both the test and predicted curves agree well during the initial portion of the pulse, up to approximately 0.015-s. After this time, the predicted response removes velocity more quickly than the test and crosses zero velocity slightly before the test response.

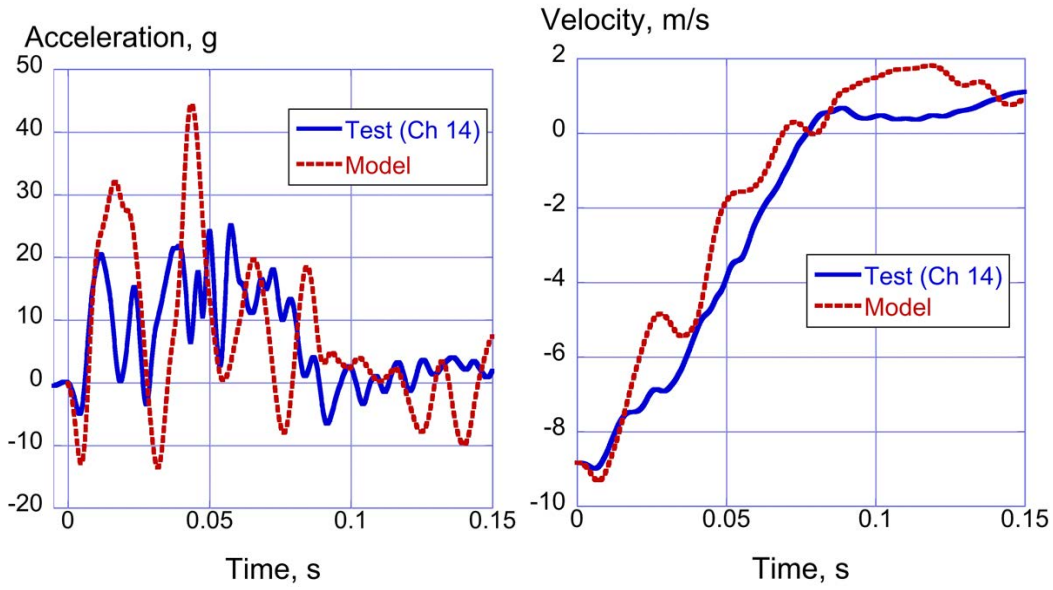

(a)Acceleration responses. (b) Velocity responses.

Figure 28. Vertical acceleration and velocity comparisons at the port window at FS 5805.

The test/analysis comparisons of vertical acceleration and velocity responses are shown in Figures 29(a) and (b), respectively, for the port aisle location at FS 5805 (see Figure 5). The test and model acceleration time histories both indicate an initial negative peak of 25-g. Subsequently, the model exhibits two peaks of 50- and 30-g, but generally matches the test response following the first large peak. The velocity responses agree well, crossing zero velocity at approximately the same time and exhibiting similar rebound responses.

The test/analysis comparisons of vertical acceleration and velocity responses are shown in Figures 30(a) and (b), respectively, for the starboard window location at FS 5805 (see Figure 5). The test

and model acceleration time histories agree very well, especially during the early part of the pulse. The simulation matches the magnitude and phase of the test oscillations, up to 0.075-s. After 0.075-s, the model over predicts the magnitude of the test acceleration curve. The velocity responses agree very well, again up to 0.075-s. After this time, the two curves deviate and the model curve crosses zero velocity earlier than the test.

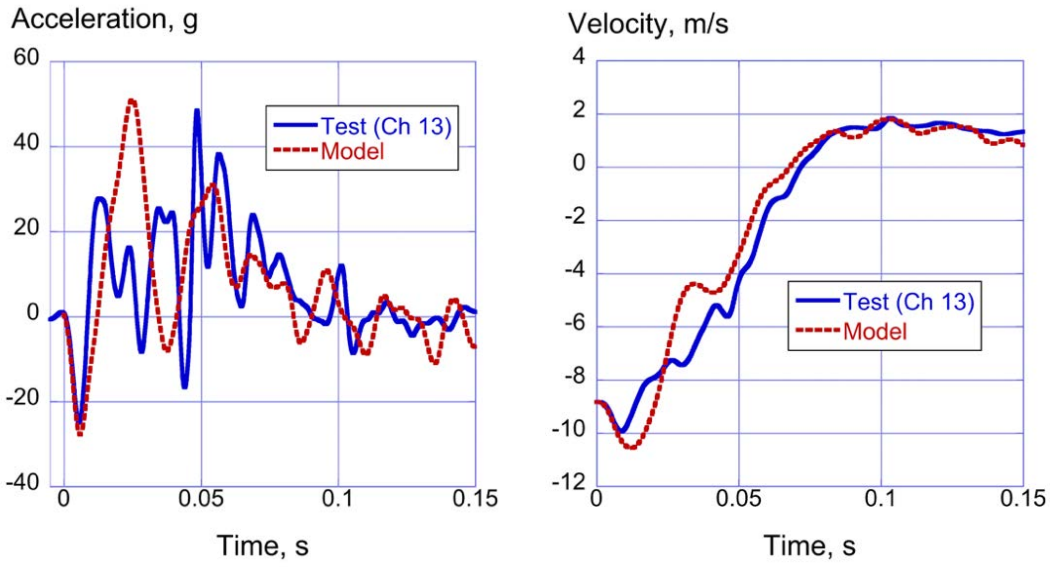

(a)Acceleration responses. (b) Velocity responses.

Figure 29. Vertical acceleration and velocity comparisons at the port aisle at FS 5805.

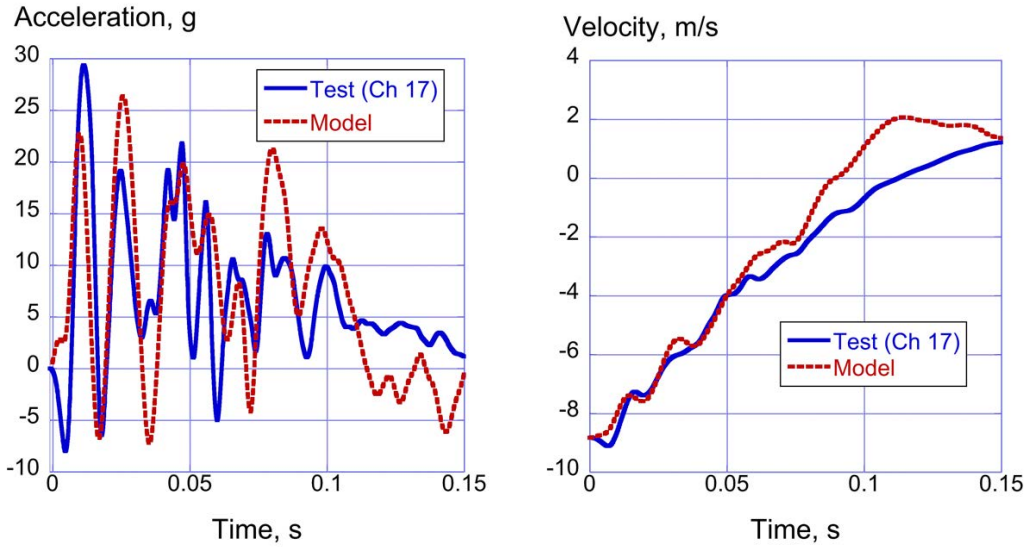

(a)Acceleration responses. (b) Velocity responses.

Figure 30. Vertical acceleration and velocity comparisons at the starboard window at FS 5805.

The test/analysis comparisons of vertical acceleration and velocity responses are shown in Figures 31(a) and (b), respectively, for the port window location at FS 6805 (see Figure 5). The model acceleration response again exhibits four peaks and matches the duration of the test response closely. The test acceleration response contains many oscillations, making it difficult to discern a definitive pulse shape. The velocity responses indicate that the model removes velocity more quickly that the test; however, both curves cross zero velocity at nearly the same time. The rebound velocity responses are different between test and model.

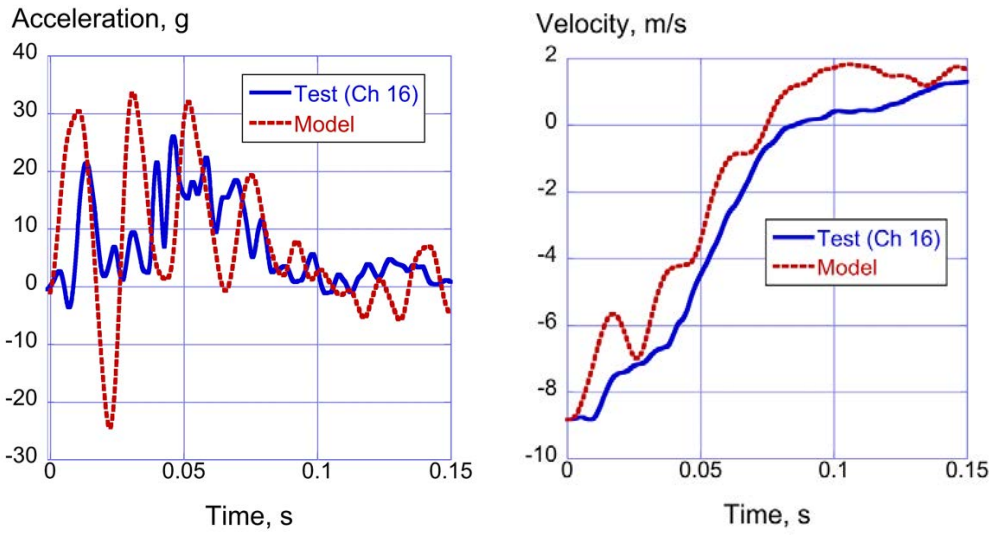

(a)Acceleration responses. (b) Velocity responses.

Figure 31. Vertical acceleration and velocity comparisons at the port window at FS 6805.

The test/analysis comparisons of vertical acceleration and velocity responses are shown in Figures 32(a) and (b), respectively, for the port aisle location at FS 6805 (see Figure 5). The level of agreement between the test and model acceleration responses is not as good as seen previously. The model exhibits a peak of 40-g at 0.04-s, and the test response exhibits a peak of 44-g at 0.056-s. Even the test and model velocity responses do not agree well. The test exhibits an initial negative velocity, which is not observed in the model response. Both curves cross zero velocity at different times and show different rebound responses.

The test/analysis comparisons of vertical acceleration and velocity responses are shown in Figures 33(a) and (b), respectively, for the starboard aisle location at FS 6805 (see Figure 5). At this location, the model acceleration response exhibits two peaks, one of 31.5-g and the second at 21-g. Once again, the test response contains many oscillations. The model crosses zero velocity sooner than the test velocity response. In addition, the model response removes velocity more quickly than the test and has a different rebound response than the test.

The test/analysis comparisons of vertical acceleration and velocity responses are shown in Figures 34(a) and (b), respectively, for the starboard window location at FS 6805 (see Figure 5). At this location, the model and test acceleration responses are similar, both responses exhibiting several peaks of similar magnitude. The velocity responses agree fairly well, with the model response removing velocity more quickly than the test and crossing zero sooner than the test. Both curves have similar rebound responses and magnitudes.

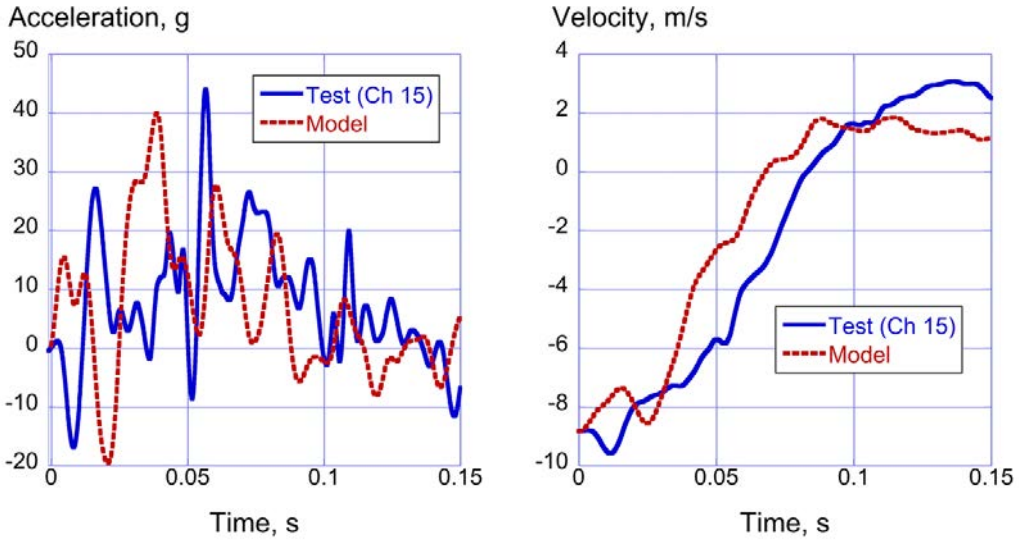

(a)Acceleration responses. (b) Velocity responses.

Figure 32. Vertical acceleration and velocity comparisons at the port aisle at FS 6805.

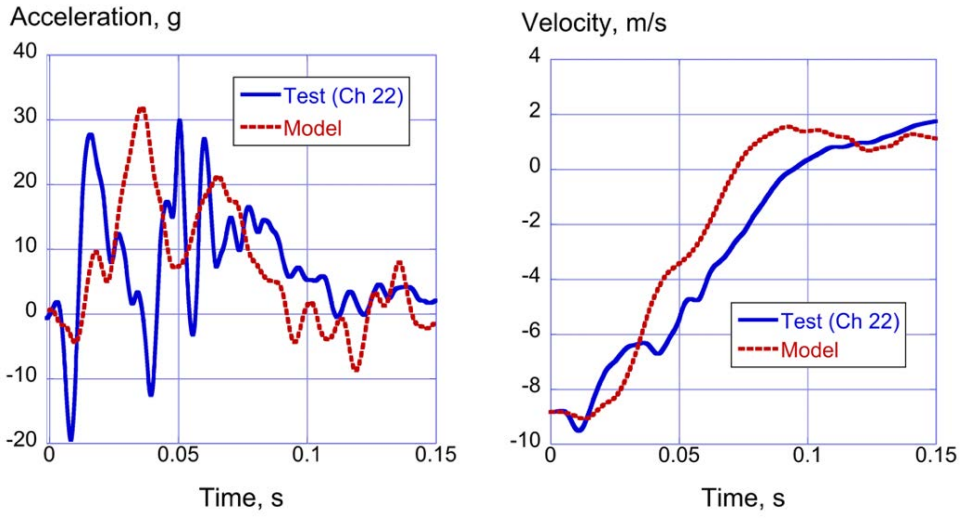

(a)Acceleration responses. (b) Velocity responses.

Figure 33. Vertical acceleration and velocity comparisons at the starboard aisle at FS 6805.

As a means of performing a more rigorous test/analysis comparison, the average acceleration was calculated for the experimental and analytical responses. The average acceleration was obtained by calculating the area under the acceleration curve from time zero to the end time of the pulse duration, and then dividing the area by the pulse duration. The pulse duration was determined as the time of maximum rebound. For the test responses, a pulse duration of 0.13-s was determined by averaging all of the individual pulse durations for each data channel. For the model, an average pulse duration of 0.128-s was calculated in a similar manner. These pulse duration values were used to determine average accelerations, which are listed in Table 6. Percentage differences between test and model data were calculated. All of the percentage differences are under 15%, indicating a good level of test/analysis agreement. Note that 5 of 7 data points are at or under 10%.

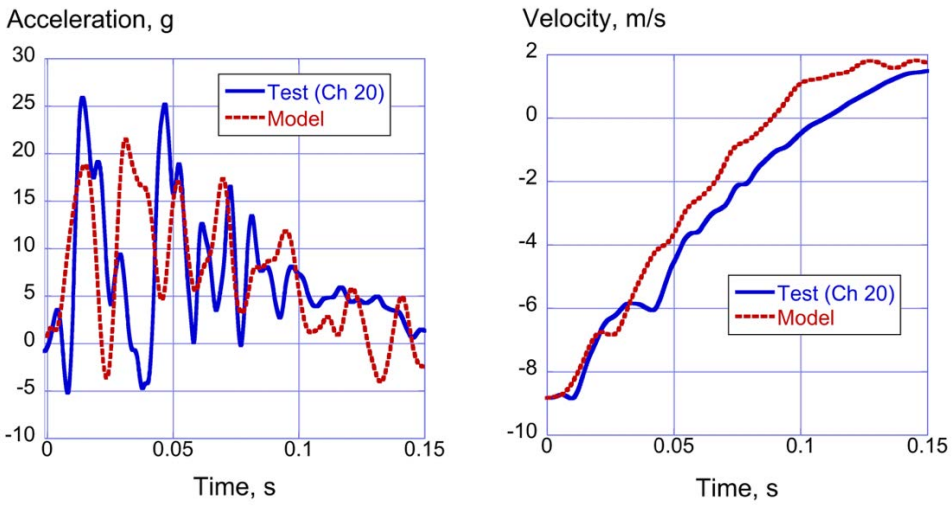

(a)Acceleration responses. (b) Velocity responses.

Figure 34. Vertical acceleration and velocity comparisons at the starboard window at FS 6805.

Table 6. Test-analysis comparisons.

Location	Avg. Acceleration, g		Percent Difference,
	Test	Model	%
Port Window at FS 5805	7.4	8.1	9.5
Port Aisle at FS 5805	8.05	8.24	2.4
Starboard Window at FS 5805	7.5	8.5	13.3
Port Window at FS 6805	7.6	8.2	7.9
Port Aisle at FS 6805	9.2	8.1	11.9
Starboard Aisle at FS 6805	7.84	7.65	2.4
Starboard Window at FS 6805	7.7	8.47	10.0

ii. Structural Deformations and Failures

A post-test photograph of the test section is shown in Figure 35(a), in which the section has been completely unloaded, including removal of the hat racks, floor panels, and luggage. Discrete

failure points at the floor level, as well as plastic deformation of the bottom centerline of the section, are evident. A picture of the model is shown at 0.038-s in Figure 35(b) without the luggage, hat racks, floor panels, and the soil impact surface. The model exhibits multiple failures of the floor support structure, especially in the central region of the floor. These failures are caused by flexure of the floor supports and pressure from the luggage. As the simulation progresses, these failures become more widespread. The test article exhibits plastic deformation and failures at the bottom centerline region, as shown in Figure 36(a). Floor-level failures include one complete separation of the seat tracks, and failures of the side-to-side floor support structure, as depicted in Figure 36(b). An impact sequence, taken from the high-speed video coverage, is shown in Figure 37. This figure depicts airframe deformation, as well as occupant flailing. Note that both the test article and the model experienced plastic deformation and failures of the lower fuselage structure between the stanchions.

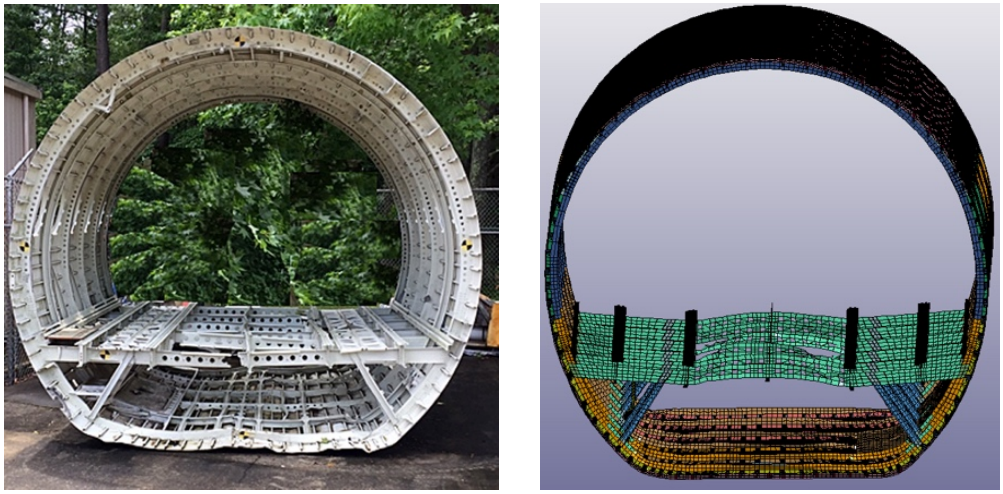

(a)Post-test photo. (b) Model photo at 0.038-s.

Figure 35. Post-test photo and model depiction at 0.038-s of the F-28 section.

(a)Bottom centerline failures. (b) Floor failures.

Figure 36. Post-test photographs.

A sequence of model deformation is shown in Figure 38 for four time steps, corresponding to the time steps shown in the test sequence (see Figure 37). The model shows excessive deformation of the luggage, indicating that the material properties used for the luggage may be inadequate. However, some luggage deformation is evident in the test sequence, shown in Figure 37. The luggage does exert an upward force on the floor support structure, which is bending due to downward seat track loading on both sides of the floor. It is interesting to note that the cargo door, which is located on the lower right side of the section when viewing the photos in Figure 37, causes asymmetry in the deformation pattern of the section. However, this effect is not seen in the model, likely due to the presence of the luggage. The cargo door and surrounding support structure were included in the model.

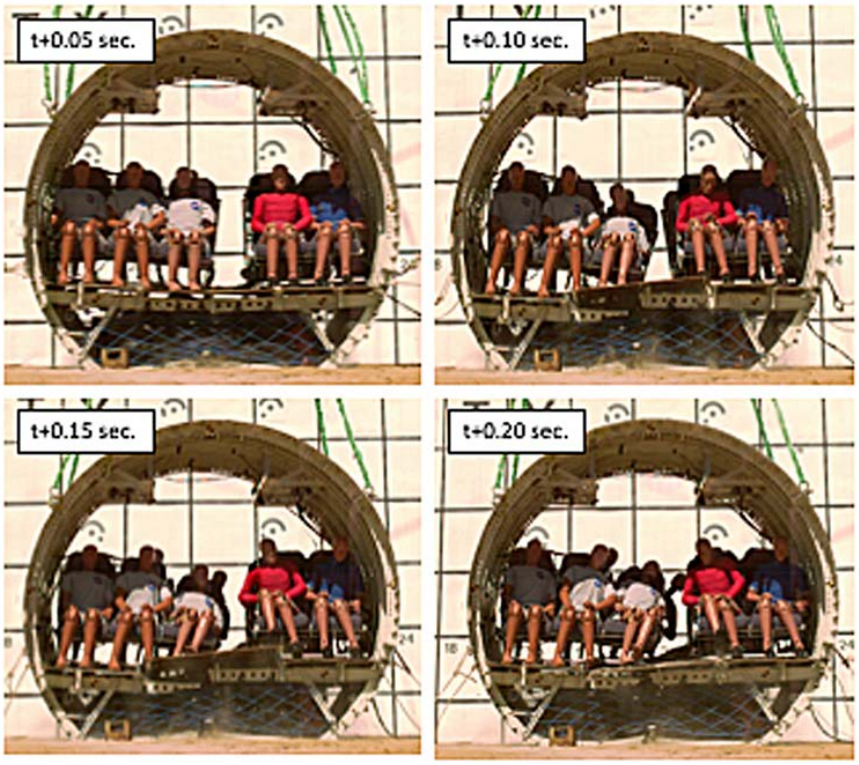

Figure 37. Impact sequence of the test.

iii. Soil Deformation

A photograph showing the crater created in the soil by the drop test of the F-28 forward section is shown in Figure 39(a). The crater measured approximately 9-ft long by 7-ft 4-in. wide. Depth measurements ranged from 0.25-in. to 1.75-in. A fringe plot of z-displacement of the soil model is shown in Figure 39(b). Since the soil was represented using properties of hard soil, the maximum predicted soil depth was 0.14-in., which is considerably less than the measured values. One explanation for the poor level of agreement may be that the soil mesh was fairly crude. In the F-28 wing-box section simulation, a much finer soil mesh was used.

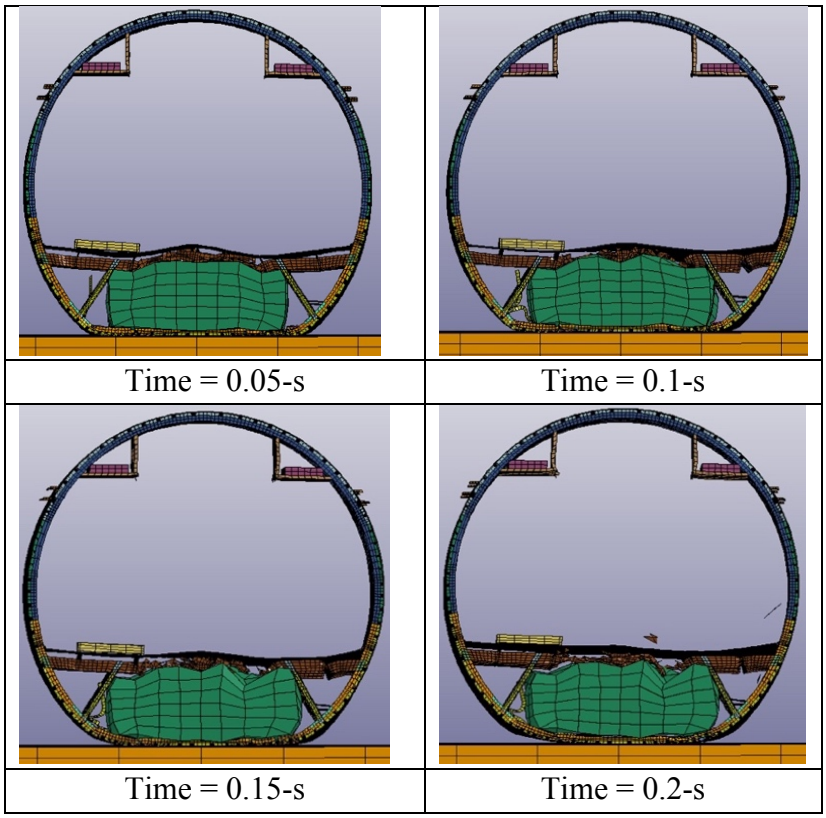

Figure 38. Model deformation sequence.

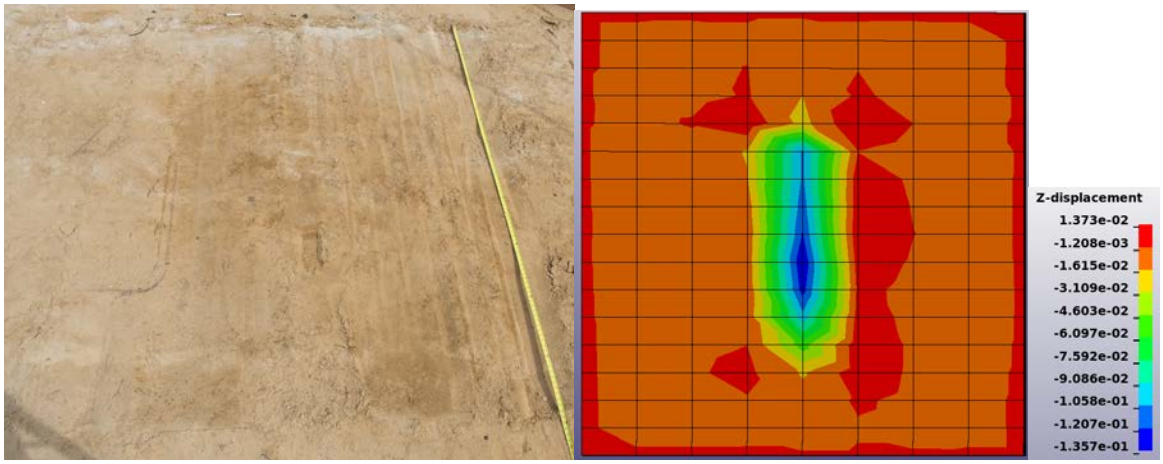

(a)Photograph of crater. (b) Fringe plot of z-displacement of soil.

Figure 39. Crater in soil created by the F-28 forward section drop test and model deformation.

iv. Seat/Occupant Simulation Results for the F-28 Forward Section

The model of the F-28 forward section that included two LSTC Detailed FEMs, 3 rigid torso surrogate models, lap belt restraints, and seats is shown in Figure 40. The finite element seat models and dummy occupant models were only included in the front row. Concentrated masses

were used to represent the seats/restraints/ATDs in the second row. The section model contained 875,000 nodes and 1.23 million elements.

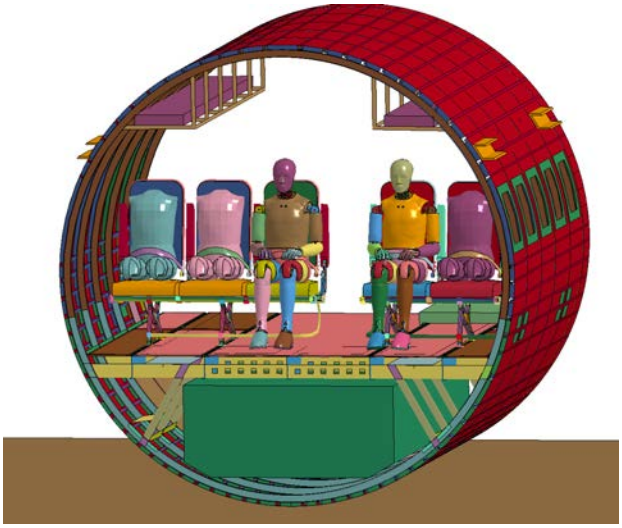

Figure 40. F-28 forward section model with ATDs and seats.

Following integration of the triple and double seats, lap belt restraints, and occupant models into the forward section model, a series of simulations was performed in which model parameters, or factors, were varied. The factors were modified to avoid runtime errors due to negative volume distortions in the foam elements, as well as to calibrate the pelvic acceleration responses with test data. These factors include:

- Airframe damage progression - The aluminum floor structure showed failure along all of the lateral floor beams in varying locations. The progression of that failure changed the floor response and therefore the loading of the seats and ATDs. Selection of the proper failure strain was critical in qualitatively and quantitatively replicating the damage progression. For the lateral shear support structure, a failure strain of 0.15 was used in the material model *MAT_PLASTIC_KINEMATIC. Also, the elements representing the luggage in the cargo hold were reduced in height by 20% to better match the timing of the luggage contact with the subfloor beams.
- Seat foam material characterization - The dynamic foam stress/strain curves were scaled up and down to account for strain rate effects. The compaction component of the stress/strain curve, at volumetric strains greater than 0.6, was artificially increased to prevent negative volumes in the foam elements.
- Hourglassing - The elements used for the seat cushion are single-point integration elements. While this element formulation is recommended for foams and soft materials, the single-point integration element causes zero-energy modes of distortion in the elements known as hourglassing. Excessive hourglassing can drastically reduce the time step or cause runtime failures. Algorithms are used to limit the hourglassing modes, and the choice of these

algorithms can adversely increase the overall energy in the model, or artificially stiffen the foam material. Type 3 hourglassing was used with a coefficient of 0.1.

- ATD positioning/preloading - The ATDs were positioned in the seats prior to the drop test with the lap belts tight on the pelvis and upper thigh. The ATDs distort the seat cushion, and create an initial stress state in the cushion. Because of the freefall after release, the ATDs unload from the 1-g stress state. However, the lumbar load data from the tests suggests that, just after release, the ATDs did not fully unload the lumbar spine. The likely source of this partial unloading was the restraining lap belt. To pre-deform the cushion and fit the lap belt, a quasi-static 1-g run was performed where the seated occupant model was constrained at the sling attachment points. As the ATD models compressed the seat cushions, an *ELEMENT_SEATBELT_RETRACTOR with 100-lb of preload was used to reduce the slack from the seat belts. At the deformed state where the ATD compressed the cushion, the new node locations of the ATDs and seats were exported. The original node locations for the impact simulation were overwritten by the new node locations. The initial stress state in the foam was also defined from the new node locations. Original node locations were redefined using *INITIAL_VOLUME_REFERENCE_GEOMETRY.
- LS-DYNA parallelization schemes - There are two options for shortening the runtime by distributing the run over multiple processors. SMP is used to distribute over processors on the same machine, but is limited in performance improvement beyond 8-12 processors. Massively Parallel Processing (MPP) can use processors over multiple nodes or within the same processor, and linearly improves runtime performance for hundreds of processors. SMP is more stable than MPP, but because of the limitation in performance, requires a longer runtime for large-scale models. MPP uses a different contact algorithm than SMP, and has consistency issues depending on the number of processors and approaches used to decompose the model domain. MPP was used for various sensitivity runs, but SMP was used for the final run of record to ensure consistency. The runtime for the 0.2-second duration impact was over 40 hours.

The predicted results for fuselage deformation and ATD motion are shown in Figure 41. The ATDs compress the seat cushion and deform the seat pan fabric. The floor and subfloor sag in the middle as the fuselage ovalizes, and the seats roll towards the centerline. For the triple seat, the cross bars begin to permanently deform at 0.030-s and the baggage bar comes into contact with the floor and deforms. Peak loading occurs right before 0.060-s, and the ATDs begin to rebound out of the seats at 0.1-s.

The pelvic acceleration responses for the LSTC Detailed FEMs on the double and triple aisle seats are plotted in Figure 42 with test data. The test results show acceleration magnitudes of 30-g for the double seat and 20-g for the triple seat. The model results indicate a much higher response, 40-g for the triple seat and 53-g for the double seat, with a sharper rise time (0.020-s) compared to the test data (0.050-s). The overall durations of the pulses are similar, at approximately 0.090-s. Despite apparent reductions in the dynamic overshoot by incorporating changes based on the

modeling factors discussed previously, the ATD loads remained higher in the model compared with test.

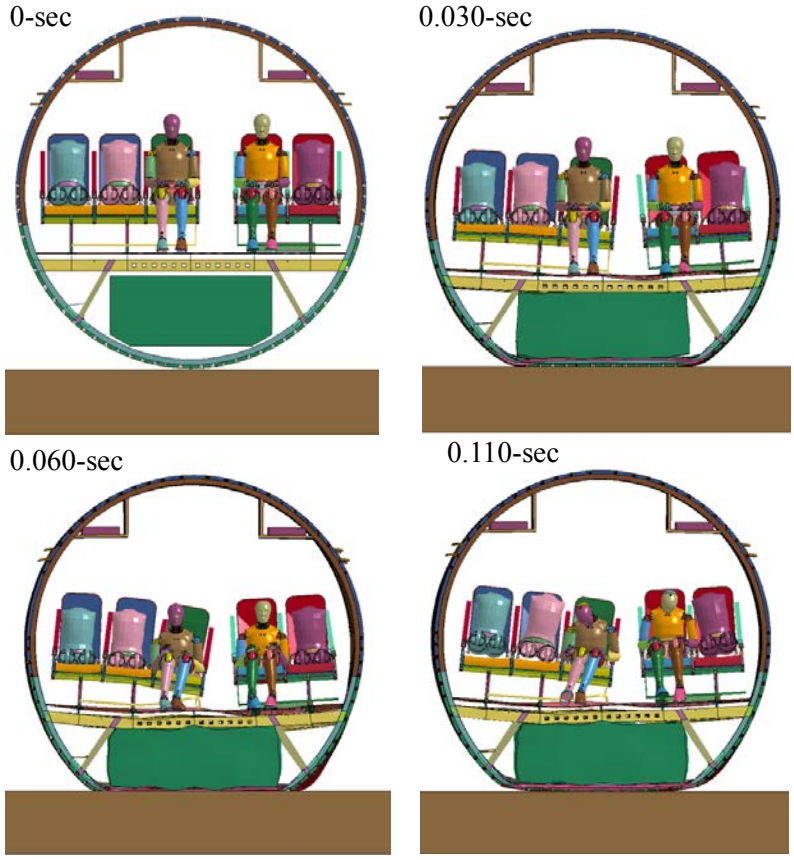

Figure 41. Forward Section FEM with ATDs and Seats- Deformation Sequence.

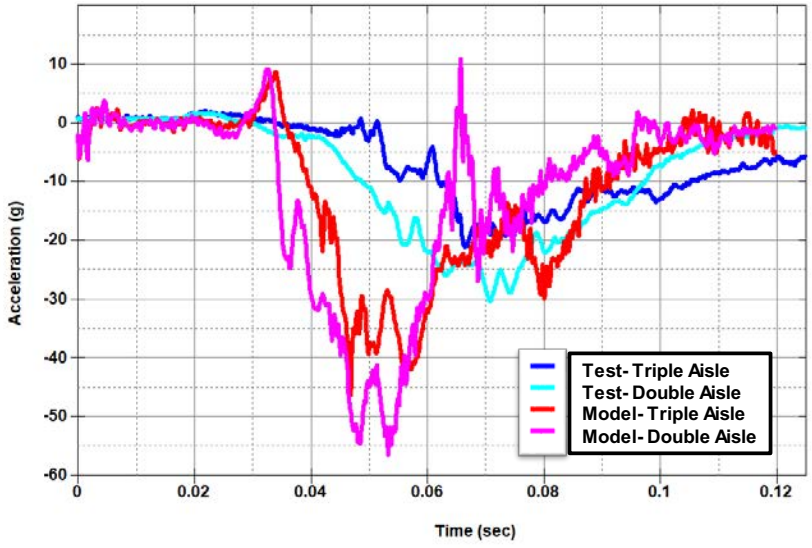

Figure 42. Pelvic z-acceleration – F-28 forward section model with seat and occupant models.

B. F-28 Wing-Box Fuselage Section

i. Acceleration Time Histories

As with the F-28 forward section, the experimental and analytical acceleration responses were both filtered using a SAE CFC 60 low-pass filter [27]. As mentioned previously, the predicted acceleration traces were output based on local coordinate systems that were defined at each concentrated mass on the seat tracks. The local coordinates can translate and rotate as the model deforms under impact loading. Thus, since these coordinate systems are not inertial systems, the data obtained using these coordinates cannot be integrated to obtain velocities or average accelerations. Therefore, no velocity comparisons are shown. Instead, plots of test-analysis forward acceleration responses are included, as well as the vertical acceleration responses. It is important to note that, in this section of the paper, the term 'vertical' refers to acceleration responses that are normal, or perpendicular, to the floor of the fuselage section. Likewise, the term 'forward' refers to acceleration responses that are parallel to the floor of the fuselage section.

The test/analysis comparison of vertical acceleration responses is shown in Figure 43 for the port window location at FS 10305 (see Figure 8). Note that the forward acceleration data at this location (Channel 17) was over ranged. The predicted vertical acceleration response matches the magnitude and shape of the test response, even though the peak acceleration of the test response is slightly under predicted by 3- to 4-g.

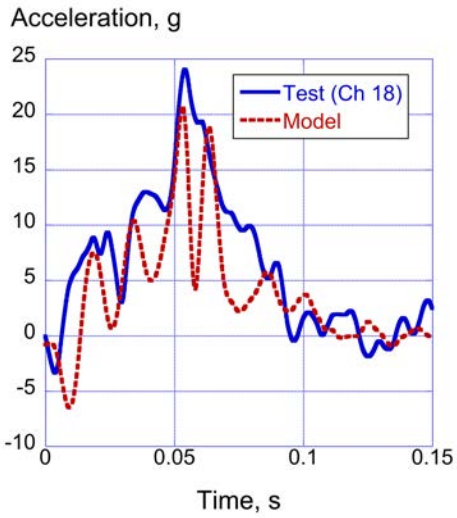

Figure 43. Vertical acceleration comparison at the port window at FS 10305.

The test/analysis comparisons of vertical and forward acceleration responses are shown in Figures 44(a) and (b), respectively, for the port aisle location at FS 10305 (see Figure 8). Once again, the predicted vertical acceleration response matches the shape of the test response; however, the magnitude is slightly under predicted. Both acceleration responses exhibit two peaks just after 0.05-s, but the predicted response is on the order of 3-g lower in magnitude. As shown in Figure

44(b), the model does a reasonably good job of predicting the magnitude and shape of the forward acceleration test response, with the exception of a sharp peak in the model response at 0.065-s, which is not seen in the test response.

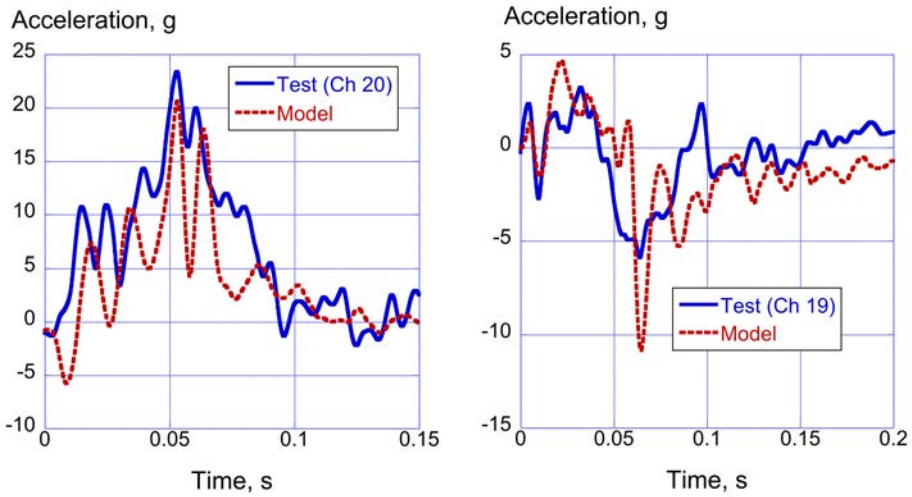

(a)Vertical acceleration responses. (b) Forward acceleration responses.

Figure 44. Vertical and forward acceleration comparisons at the port aisle at FS 10305.

The test/analysis comparisons of vertical and forward acceleration responses are shown in Figures 45(a) and (b), respectively, for the starboard aisle location at FS 10305 (see Figure 8). The predicted acceleration response matches the overall shape of the test acceleration response, but under predicts the magnitude more dramatically. For example, the test response exhibits a peak of 26.7-g at 0.056-s. In comparison, the predicted peak acceleration is 16.9-g at 0.062-s, a difference of almost 10-g. The comparison of forward acceleration responses is good; however, once again, the model exhibits a sharp peak at 0.065-s that is not seen in the test response.

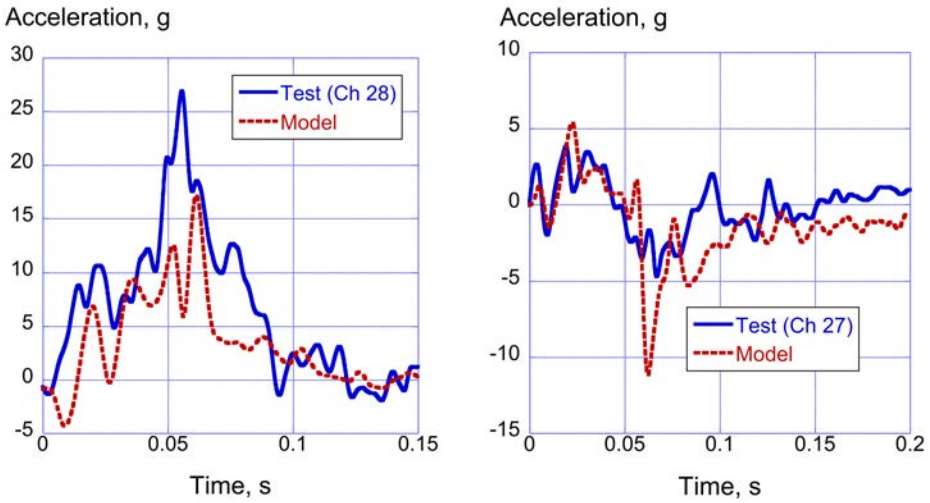

(a)Vertical acceleration responses. (b) Forward acceleration responses.

Figure 45. Vertical and forward acceleration comparisons at the starboard aisle at FS 10305.

The test/analysis comparison of vertical acceleration responses is plotted in Figure 46 for the starboard window location at FS 10305 (see Figure 8). Once again, the predicted vertical acceleration response matches the shape of the test response, but under predicts the magnitude. As an example, the test peak acceleration is 28.9-g at 0.055-s, whereas the predicted peak is 15.7-g at 0.06-s, a difference of 13.2-g. Data from Channel 25 were over ranged and model comparisons for forward acceleration are not shown.

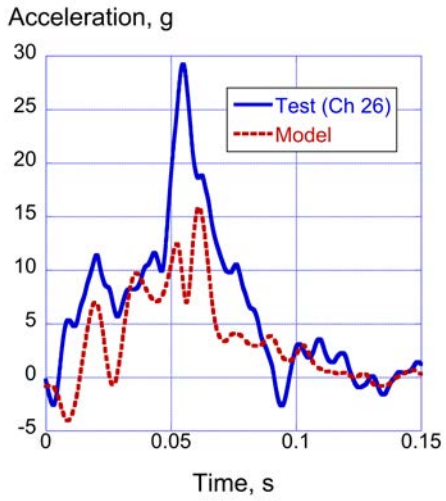

Figure 46. Vertical acceleration comparisons at the starboard window at FS 10305.

The test/analysis comparisons of vertical and forward acceleration responses are shown in Figures 47(a) and (b), respectively, for the port window location at FS 10790 (see Figure 8). The vertical acceleration responses exhibit multiple oscillations, making it difficult to discern a pulse shape. The predicted peak acceleration is 19.1-g at 0.027-s, whereas the test peak is 18.2-g at 0.054-s. The pulse duration is well predicted. The model, once again, agrees well with the forward acceleration test response, this time even matching the peak response that occurs at 0.065-s.

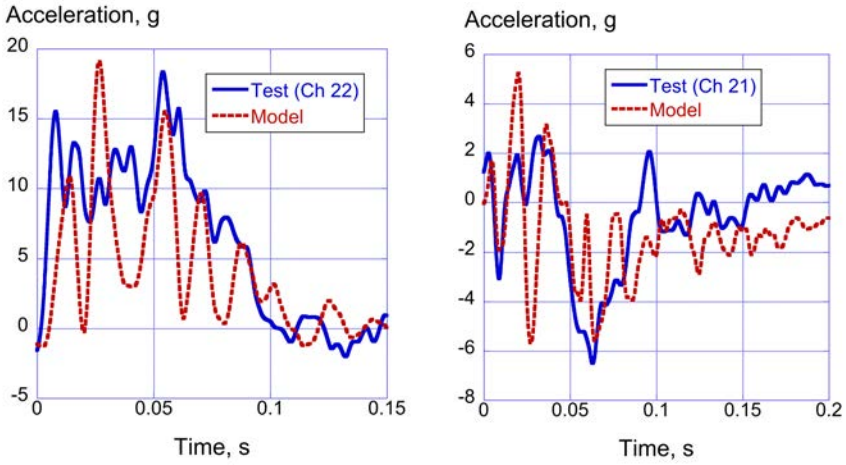

(a)Vertical acceleration responses. (b) Forward acceleration responses.

Figure 47. Vertical and forward acceleration comparisons at the port window at FS 10790.

The test/analysis comparison of vertical acceleration responses is shown in Figure 48 for the port aisle location at FS 10790 (see Figure 8). The test vertical acceleration response contains many oscillations making it difficult to discern a pulse shape. The predicted response also contains many oscillations, of roughly the same magnitude as the test. In addition, both responses have similar pulse durations. Channel 23 data were over ranged and, therefore, no comparison plot is available.

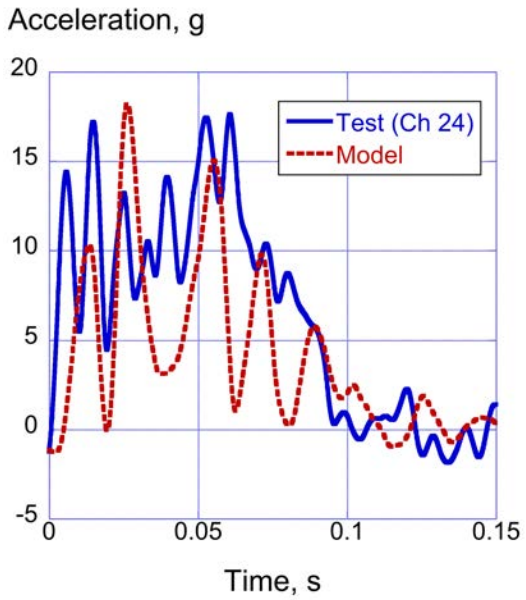

Figure 48. Vertical acceleration comparison at the port aisle at FS 10790.

The test/analysis comparisons of vertical and forward acceleration responses are shown in Figures 49(a) and (b), respectively, for the starboard aisle location at FS 10790 (see Figure 8). The predicted vertical acceleration response matches the overall shape of the test response; however, the magnitude of the response is under predicted. The test response has a peak of 22.9-g at 0.056-s, whereas the model peak is 12-g at 0.054-s, a difference of 10.9-g. Better comparisons are seen for the forward acceleration responses, shown in Figure 49(b). The model matches the oscillatory response of the test curve and slightly over predicts the acceleration peak at 0.065-s.

The test/analysis comparisons of vertical and forward acceleration responses are shown in Figures 50(a) and (b), respectively, for the starboard window location at FS 10790 (see Figure 8). Once again, the predicted response generally matches the shape of the test curve; however, the magnitude of the response is significantly under predicted. For example, the magnitudes of the two experimental peak accelerations are 17- and 24-g. In comparison, the magnitudes of the two predicted peak accelerations are 14- and 12.5-g. The forward acceleration response compares more favorably. The model response matches the initial oscillatory test response, but again exhibits a sharp peak at 0.065-s that is not seen in the test response.

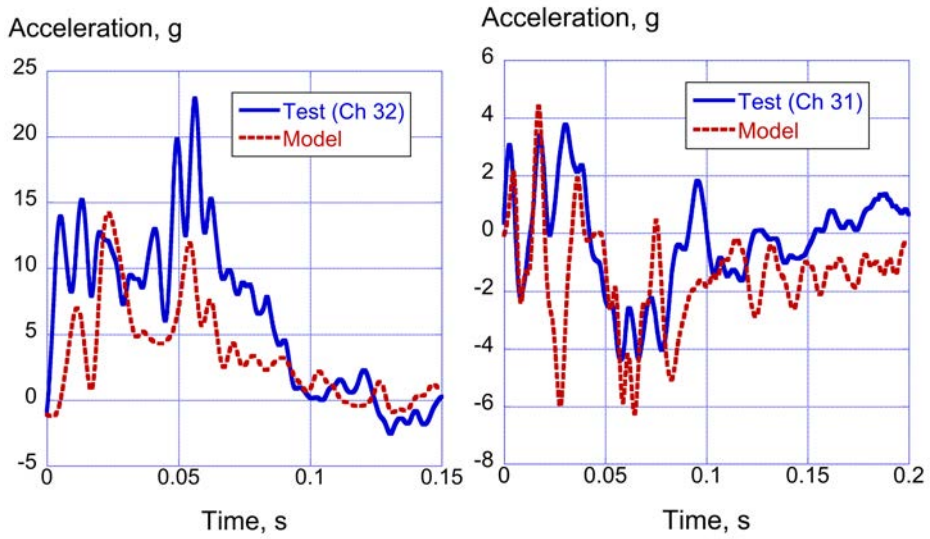

(a)Vertical acceleration responses. (b) Forward acceleration responses.

Figure 49. Vertical and forward acceleration comparisons at the starboard aisle at FS 10790.

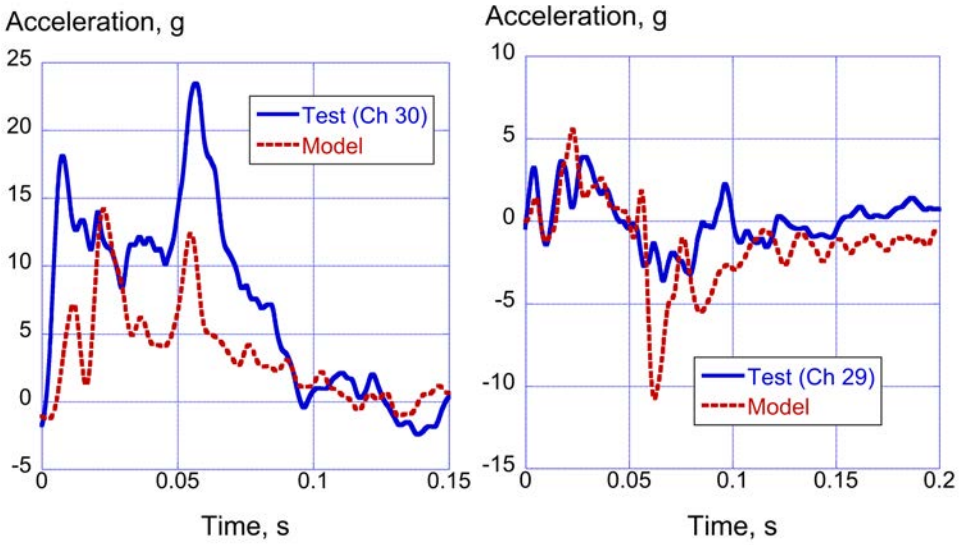

(a)Vertical acceleration responses. (b) Forward acceleration responses.

Figure 50. Vertical acceleration and velocity comparisons at the starboard window at FS 10790.

ii. Structural Deformations and Failures

Front- and rear-view photographs of the post-test F-28 wing-box section are shown in Figures 51(a) and (b), respectively. By examining the front view, it is difficult to observe any regions of structural damage. However, the rear-view shows damage that occurred in the lower cavity. This damage is highlighted in Figure 52, which shows buckling and tearing of a metal beam and failure of a lower frame. Deformation, yielding and failure of the beams located in the lower cavity of the model are depicted in Figure 53 near the end time of the simulation. Please note that the beams

are shown in a prismatic format. This picture shows twisting of the beam cross-sections and buckling of the diagonal beams under compressive loading.

(a)Front view. (b) Rear view.

Figure 51. Two post-test photographs of the F-28 wing-box section.

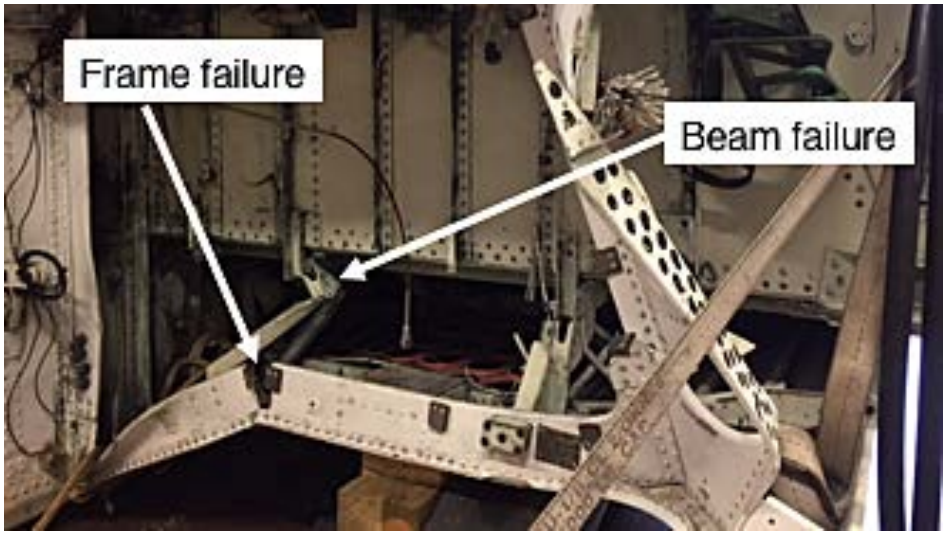

Figure 52. Close-up photograph showing damage to the F-28 wing-box section.

Next, two impact sequences are shown for both the test and the model. The first sequence, illustrated in Figure 54, shows the front view of the airframe and it highlights three significant events: impact (time = 0.0-s), the time of slap down following airframe rotation (time = 0.056-s), and the time of maximum ATD vertical displacement (time = 0.073-s). A second impact sequence is shown in Figure 55 (side view) for the same three impact events. Note that little or no deformation of the fuselage section is visible.

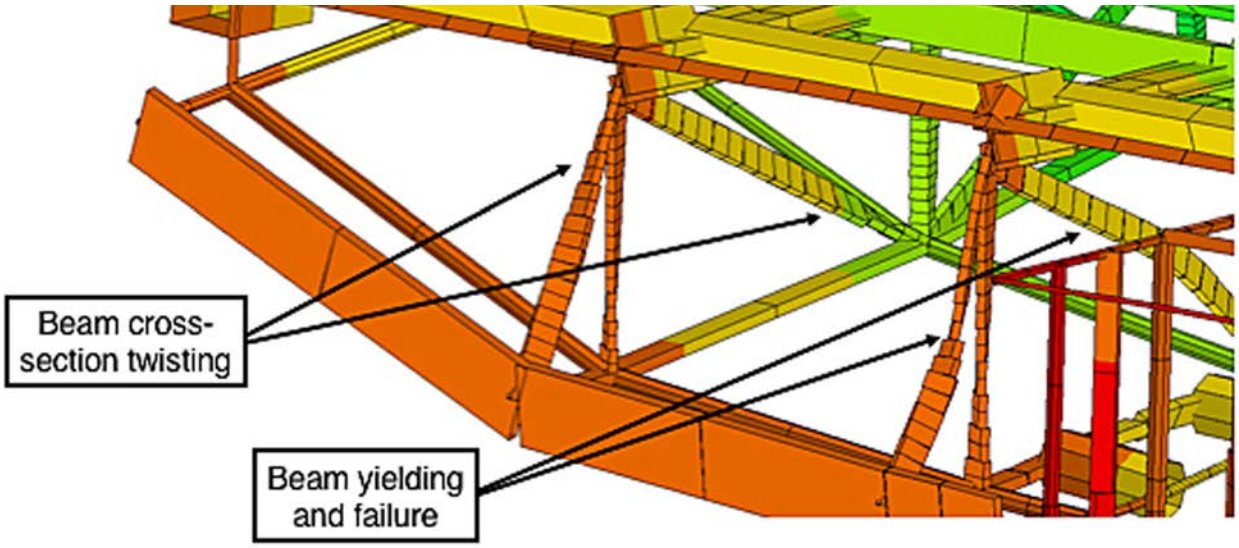

Figure 53. Beam element deformation, yielding and failure in the lower cavity.

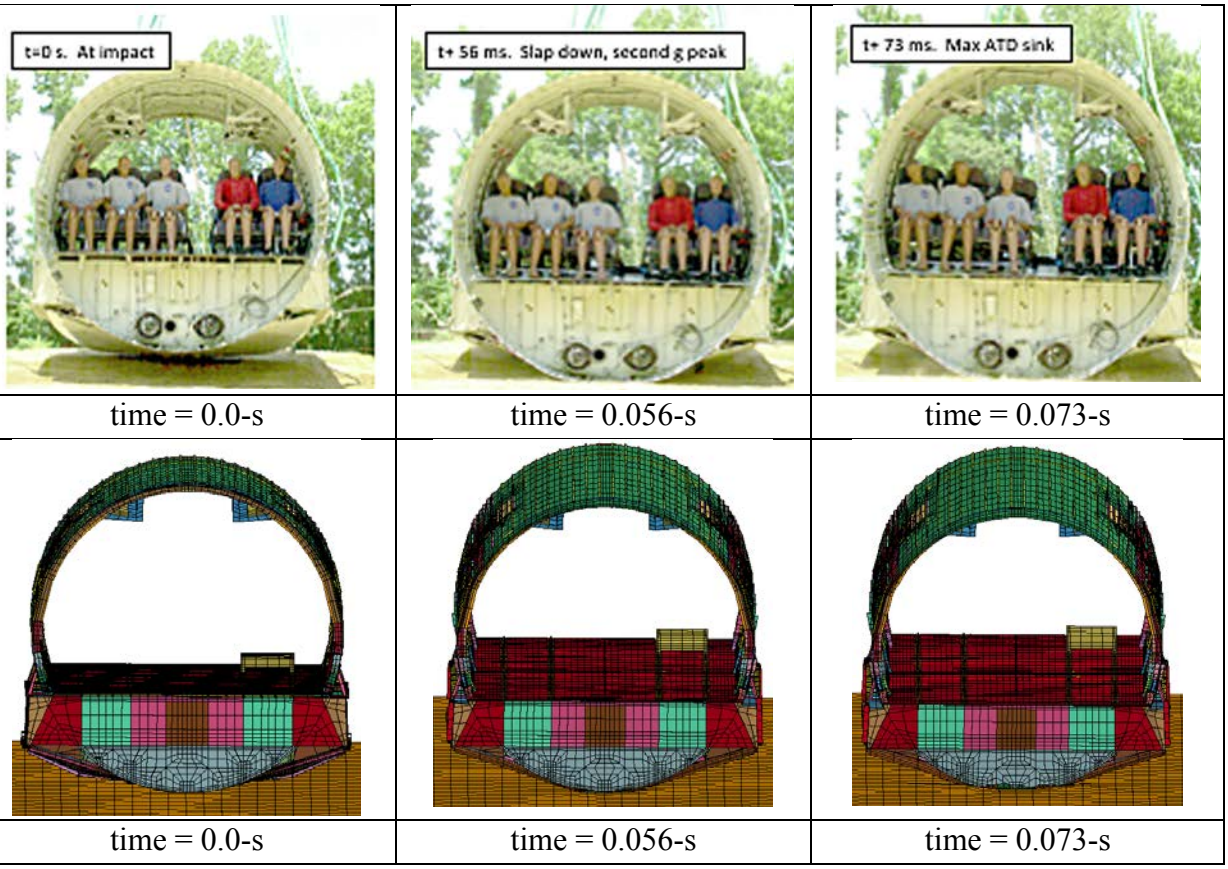

time = 0.0-s	time = 0.056-s	time = 0.073-s
time = 0.0-s	time = 0.056-s	time = 0.073-s

Figure 54. Test-analysis impact sequence (front view).

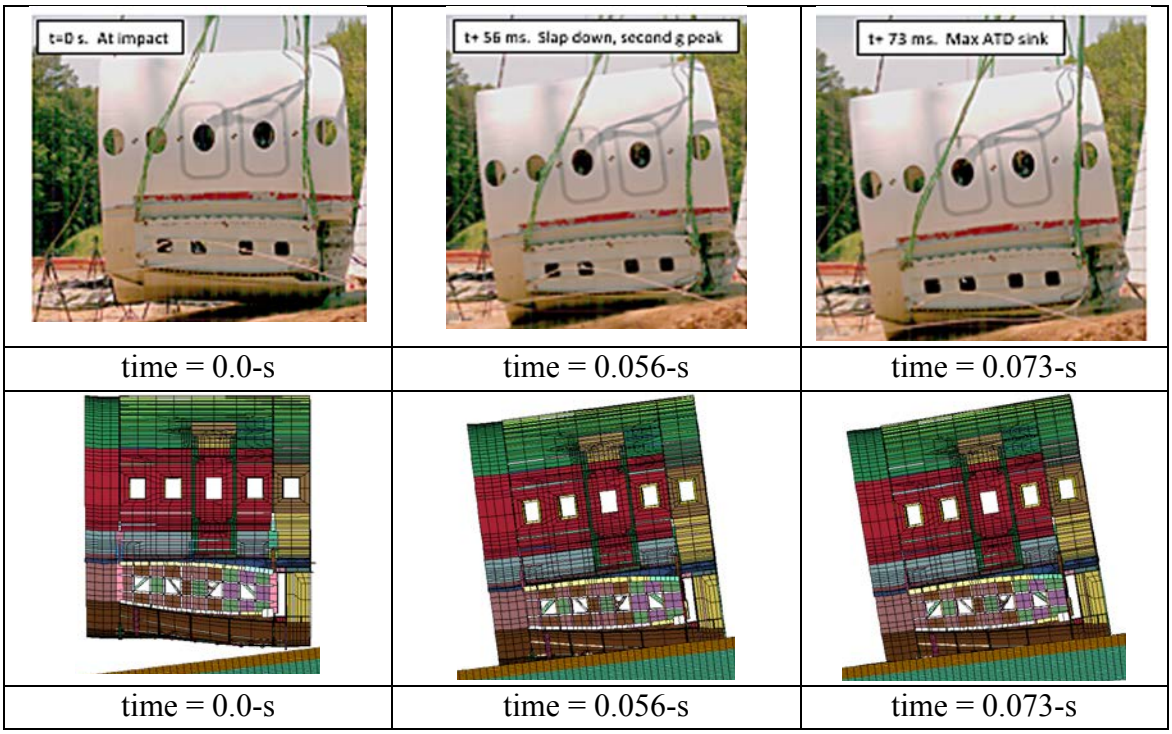

Figure 55. Test-analysis impact sequence (side view).

iii. Soil Deformation

The crater made in the GUS soil following impact of the F-28 wing-box section is shown in Figure 56. A maximum soil depth of 8-in. was measured at the initial impact location. Soil depths decrease with the distance away from the initial impact location, as indicated in Table 7. The two parallel lines evident in Figure 56 were created by two fore-aft beam supports, located on the bottom of the section. These beams tended to dig into the soil, leaving the visible marks shown in Figure 56.

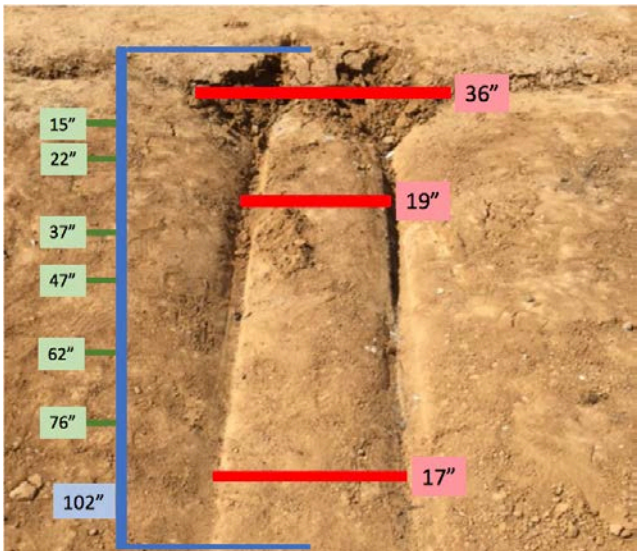

Figure 56. Photograph of soil crater following the wing-box section drop test.

Table 7. Soil depth measurements of the crater shown in Figure 56.

Distance from the top, in.	Depth (left side), in.	Depth (middle), in.	Depth (right side), in.
15	7	4.25	7.25
22	8	4	7
37	8	4	8
47	6	3.25	7.5
62	6	2.5	6
76	4.75	2.75	5.25
102	3	3	3

A fringe plot of vertical (z) displacement is shown in Figure 57. This plot is taken near the end time of the simulation and shows a large amount of displacement (7.959-in.) at the point of section slap down. This behavior is not seen in the test; however, the overall shape of the soil deformation pattern matches the test response, shown in Figure 56, well.

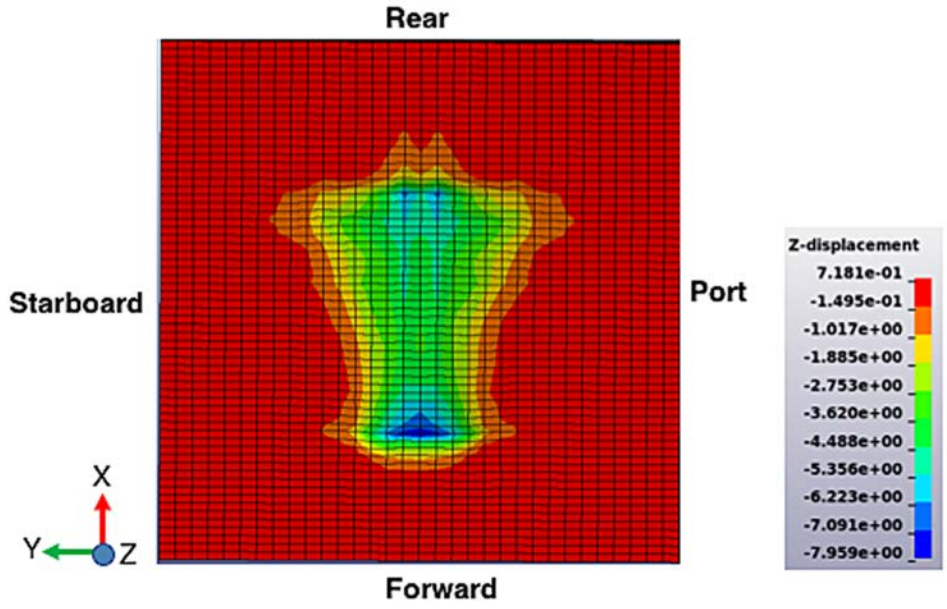

Figure 57. Fringe plot of z-displacement of the soil model from the wing-box simulation.

iv. Seat/Occupant Simulation Results for the F-28 Wing-Box Section

Major findings from the test-analysis comparison of the F-28 wing-box simulation are that the model under predicted the magnitude of the measured vertical acceleration responses at seat/floor attachment locations. Generally, the overall shape and duration of the vertical acceleration responses were well predicted; however, the magnitudes of the responses differed by as much as 10- to 14-g. Comparisons of the forward acceleration responses at these locations showed better overall agreement, with the exception that the model response often contained a sharp peak at

0.065-s that was not seen in the experimental data. One potential explanation for the poor level of agreement was that concentrated masses were used to represent the inertial properties of the seats, restraints and ATDs. Unfortunately, concentrated masses do not accurately represent the load path provided by seated and restrained dummies. Consequently, a model was executed in which one row of seats were modeled, along with one LSTC Detailed FEM representing a Hybrid III ATD, and four rigid dummy torso blocks.

A depiction of the F-28 wing-box section model with one row of seats is shown in Figure 58. One detailed LSTC Detailed FEM occupant model was placed in the aisle seat on the port side of the section. This dummy model contains roughly 405,000 nodes. The four additional seats were occupied by rigid dummy torso blocks. A depiction of just the seats and dummy models is shown in Figure 59. Note that the second row of seats and dummies was represented using concentrated masses.

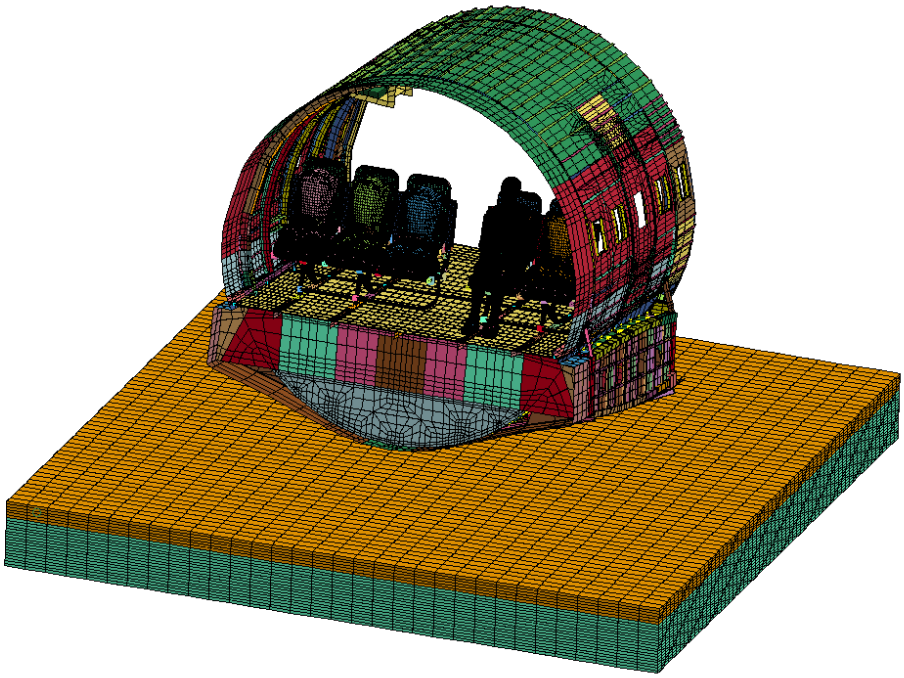

Figure 58. F-28 wing-box section model with one row of seats and dummy models.

As shown in Figure 59, the rigid dummy torso blocks and the LSTC Detailed FEM were secured to the seats using lap belt constraints. The rigid dummy torso blocks weighed 150-lb each, whereas the LSTC Detailed FEM weighed 180-lb. Both the triple and double seats were attached to the seat tracks at four locations using Constrained Nodal Rigid Bodies (CNRBs). For this model, the cushions were assigned material type 57 or *MAT_LOW_DENSITY_FOAM and the material model was calibrated based on ball penetrometer drop tests. As with the previous F-28 wing-box model, local coordinate systems were defined at the seat attachment locations.

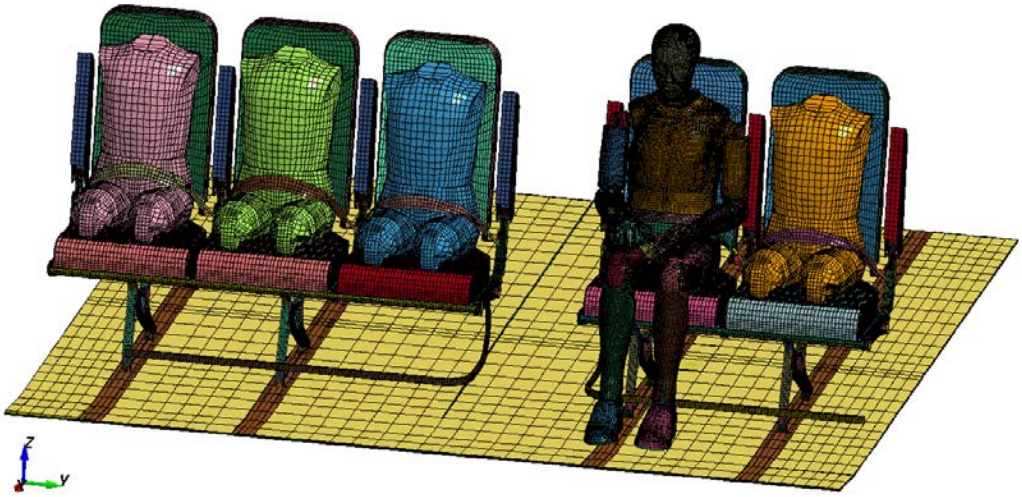

Figure 59. Picture of the single row of seats, one detailed ATD model, and rigid dummy blocks.

The finite element model, shown in Figure 58, contains: 871 parts; 93 materials; 219 CNRBs; 1 initial velocity card; 5 separate contact cards; 544,636 nodes; 7,774 beam elements; 186,233 shell elements; and, 215,000 solid elements. The model was executed for a termination time of 0.12-s and required 180 hours and 45 minutes to execute on LS-DYNA SMP Version 971 double precision, on 16 processors of a workstation computer. Output requests included local vertical and forward acceleration time history responses at the seat/seat track interfaces.

As a reminder, the instrumentation layout on the floor of the F-28 wing-box section is shown in Figure 60. Since only one row of seats and dummies were modeled, the shaded region in Figure 60 indicates the locations of channels where test-analysis comparisons are made.

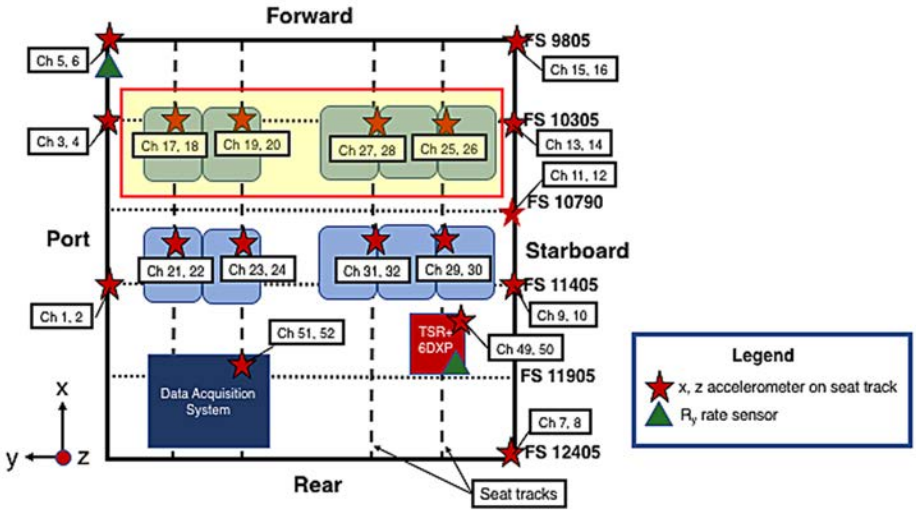

Figure 60. F-28 wing-box section floor-level instrumentation layout. For the simulation with seats and dummies, only the shaded region is used for test-analysis comparisons.

A test-analysis comparison plot of vertical acceleration at the port window location at FS 10305 is shown in Figure 61. For this plot, the results of the simulation in which the seats and dummies were modeled as concentrated masses are included (red dashed line) along with the test response (solid blue line) and the results of the simulation including seats and dummies (dashed green line). One finding is immediately apparent. Instead of under predicting the vertical acceleration peak, the model with seat and dummies now over predicts the test acceleration peak. In general, the shape and duration of the test response is well predicted by the model with seat and dummies. Note that the forward acceleration (Channel 17) was over ranged and so no comparison is made.

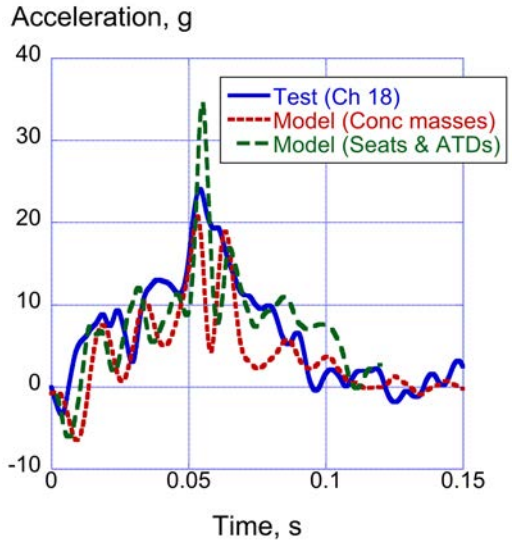

Figure 61. Comparison plot of vertical acceleration for the port window location at FS 10305.

Test-analysis comparison plots of vertical and forward acceleration at the port aisle location at FS 10305 are shown in Figures 62 (a) and (b), respectively. Once again, the model with seats and dummies over predicts the peak acceleration of the test response, but generally matches the shape and duration of the test pulse quite well. The forward acceleration response of the model with seats and dummies has eliminated the sharp spike in the response of the model with concentrated masses that occurs at 0.065-s.

Test-analysis comparison plots of vertical and forward acceleration at the starboard aisle location at FS 10305 are shown in Figures 63 (a) and (b), respectively. Once again, the model with seats and dummies now only slightly over predicts the peak acceleration of the test response, but generally matches the shape and duration of the test pulse well. The forward acceleration response of the model with seats and dummies has eliminated the sharp spike in the response of the model with concentrated masses that occurs at 0.065-s. In general, the model with seats and dummies does a better job of matching the shape and duration of the forward acceleration test response.

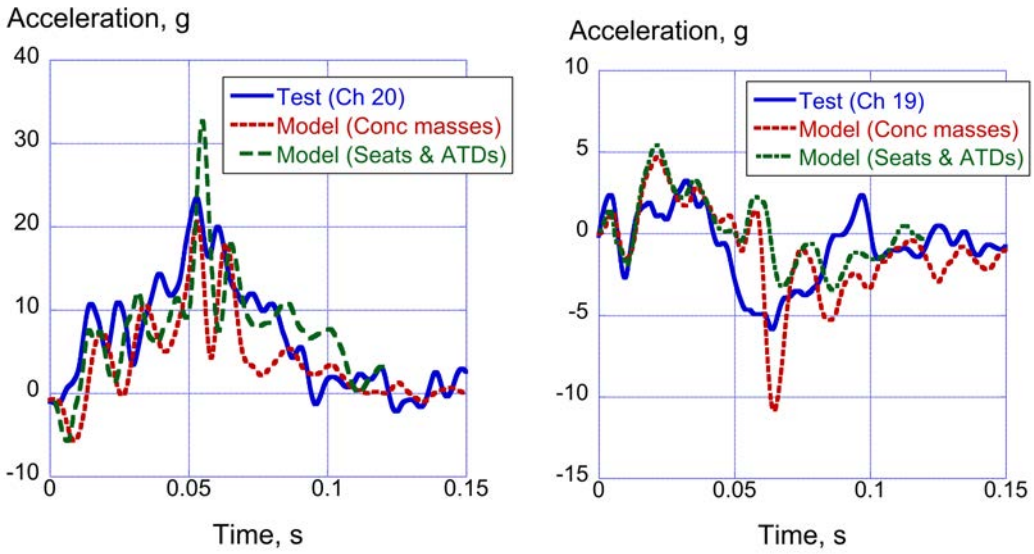

(a)Vertical acceleration. (b) Forward acceleration.

Figure 62. Plots of vertical and forward acceleration for the port aisle location at FS 10305.

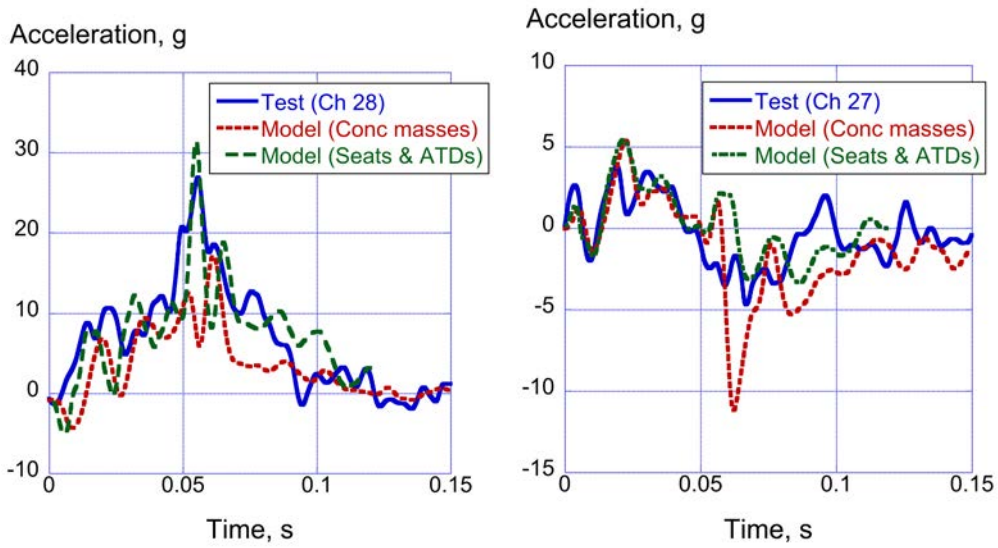

(a)Vertical acceleration. (b) Forward acceleration.

Figure 63. Plots of vertical and forward acceleration for the starboard aisle location at FS 10305.

A test-analysis comparison plot of vertical acceleration at the starboard window location at FS 10305 is shown in Figure 64. Note that the data for the forward acceleration (Channel 25) was over ranged. At this location, the predicted response of the model with concentrated masses under predicted the test acceleration peak significantly (29.5-g for the test peak compared with 15.5-g for the model, a difference of 14-g). The model with seats and dummies slightly over predicted the test peak by 2-g and matched the timing of the peak exactly. Generally, the model response matched the shape and duration of the test response well.

The results of this model revision indicate that changes to the model to better represent the physical characteristics of the test article result in improved test-analysis comparisons. While representing the inertial properties of the seats and dummies as concentrated masses was expedient, it resulted in a loss of accuracy and fidelity in the model.

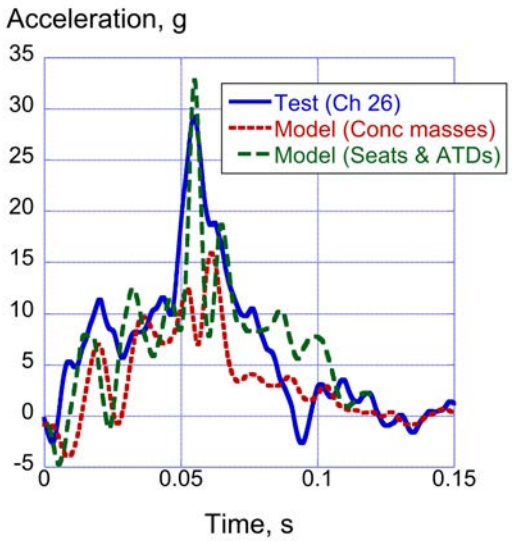

Figure 64. Comparison plot of vertical acceleration for the starboard window location at FS 10305.

The wing-box model with seats and ATDs is shown in Figure 65. With the dynamic overshoot behavior in the ATDs evident in the forward section model, only one detailed ATD was included in the wing-box section model to shorten the runtime and allow more sensitivity runs to be conducted. The model contains 537,000 nodes and 695,000 elements.

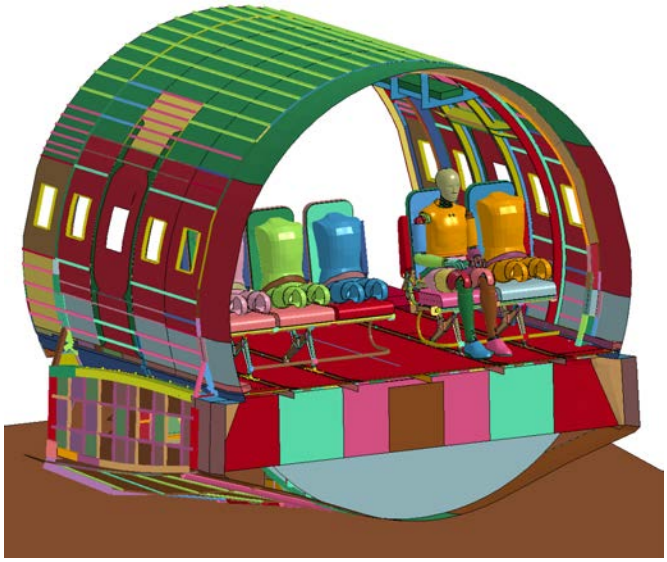

Figure 65. Wing-box section model with seats and ATD models.

A time sequence of fuselage deformation and ATD motion is shown in Figure 66. There is minimal permanent deformation in the airframe. The peak loading in the LSTC Detailed FEM occupant model occurs at 0.060-s as the front end of the fuselage contacts the soil surface. The forward deceleration causes the head to flail in extension, starting at 0.090-s.

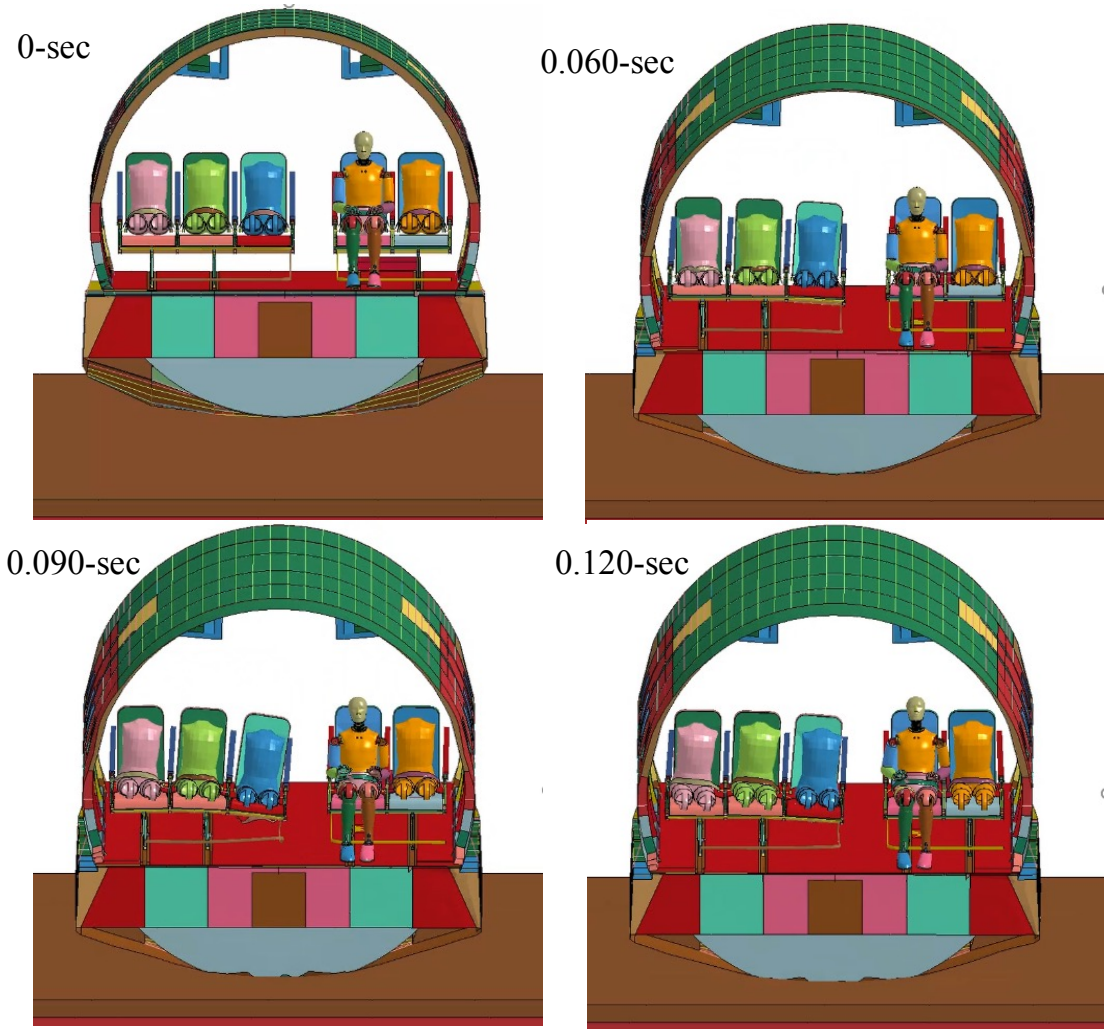

Figure 66. Deformation sequence of the combined F-28 wing-box section model.

The pelvic acceleration response of the LSTC Detailed FEM on the double aisle seat is shown in Figure 67 along with the test response. The behavior of the ATD model is similar to the forward section model with seats and ATDs. The results show peak acceleration magnitudes of 25-g for test and 45-g for the model. Again, the model shows a sharper rise time (0.020-s) compared to the test data (0.050-s). The overall durations of the pulses are similar, around 0.090-s. Because the wing-box section did not deform significantly, the source of the modeling error is likely relegated to the seat cushion or the ATD pelvic section. More studies are required to isolate those effects.

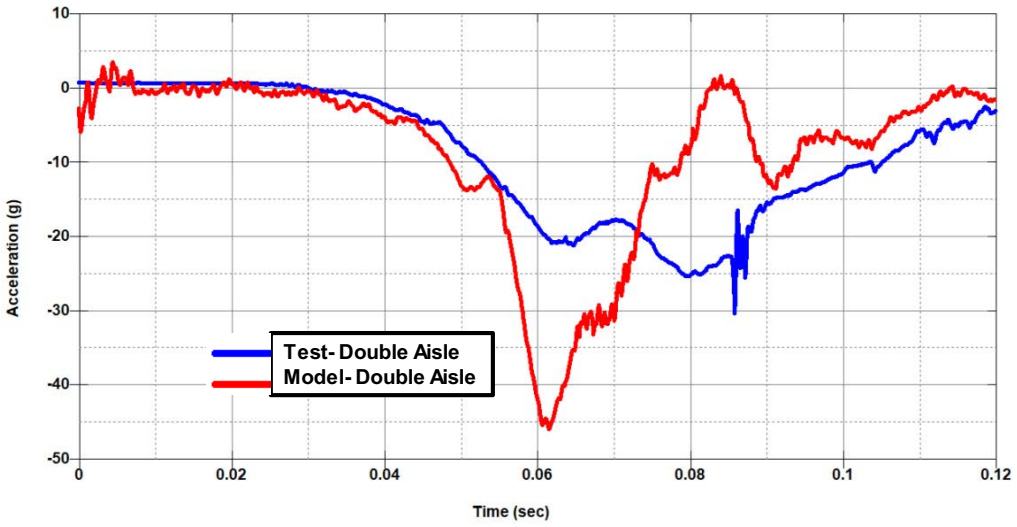

Figure 67. Pelvic z-acceleration of the LSTC Detailed FEM occupant model compared with test data.

VI. DISCUSSION OF RESULTS

This paper has presented the results of finite element simulations of vertical drop tests of two F-28 fuselage sections: a forward section and a wing-box section. The focus of the test/analysis comparisons was on seat track responses, structural deformations and failures, soil deformation, and ATD responses. For the forward fuselage section, percentage differences in average accelerations between the test and predicted responses showed that all values are under 15%, indicating a good level of test/analysis agreement. Note that 5 of 7 data points are at or under 10%. More exacting means of test-analysis comparison were not attempted. However, a new metric for quantifying test/analysis comparisons for model validation needs to be developed and utilized. Note that this same approach was not used for the wing-box section results, due to the fact that the section impacted a 10° sloped soil surface and rotated under gravitational loads. Floor-level acceleration responses were output using local coordinate systems defined at each mass location. These non-inertial coordinate systems can deform and move with the airframe under dynamic loading. Therefore, data obtained from the local coordinate systems cannot be used to integrate accelerations to obtain velocity responses or average accelerations.

For filtered acceleration time histories, the level of agreement can be determined by comparing the onset rate, magnitude, timing and overall shape of the acceleration response. Rarely will the analyst see "good" correlation between test and analysis in the sense of an absolute match for these parameters. In general, the level of correlation is deemed "good or reasonable" if these parameters are within ±20%. Thus, the need to re-evaluate the current crash data analysis and correlation methodologies for use with detailed finite element model simulations has been identified. A project was initiated at NASA Langley to better quantify the accuracy of crash simulation results.

The motivation for the project, as stated in Reference 29, was "to document modeling improvements, to evaluate design configurations analytically, and to enable certification or qualification by analysis." A conclusion of this reference was that continued work is needed to automate rigorous test-analysis correlation methodologies to improve and redefine the level of accuracy.

A. Modeling Uncertainty

For models of this size and complexity, it is useful to document some of the approximations and assumptions used in the finite element models. These are listed, as follows:

- Rivets, doublers, cutouts, and other detailed features of the airframe structure were not included in the finite element model and were instead accounted for by using average thicknesses.
- Lumped masses: Initially, seats and occupants were simulated as lumped masses that were attached to seat tracks on the floor using rigid connections. This approximation is crude as the test dummies are free to move within a limited range, thus changing the load path on the floor. Additional simulations were performed in which models of the seats, restraints, and dummies were included. The results of this model revision indicate that changes to the model to better represent the physical characteristics of the test article result in improved test-analysis comparisons. While representing the inertial properties of the seats and dummies as concentrated masses was expedient, it resulted in a loss of accuracy and fidelity in the model.
- The soil bed was represented as homogeneous within each layer. Cone penetrometer data showed some scatter in soil bearing strength with depth. Moisture in the soil changes its properties considerably. Soil properties were determined on the day of the test. While soil characterization testing was ongoing, people were walking on the soil bed to access and secure the test article. This disturbance of the soil can alter its top-layer properties due to compaction.
- Luggage properties were initially obtained from a quasi-static load test performed in 2002 of four pieces of stacked luggage. The luggage was packed with clothing, shoes, and other toiletry items. Based on the results of the forward section simulation, the luggage material properties are likely inaccurate. Subsequently, dynamic drop testing of packed luggage was performed, which confirmed this finding (see Reference 17).
- Following best practices for modeling and simulation, a mesh discretization study should have been performed. However, given the limited amount of time for model development, a mesh discretization study was not performed. The influence of mesh discretization was observed in the prediction of soil crater depth. For the F-28 forward section, a coarse mesh was used to represent the soil and poor soil depth comparisons with test data were obtained. For the F-28 wing-box section, a much finer soil mesh was used, which yielded accurate prediction of the soil crater depth.

B. Model Calibration of Time History Responses

Many approaches are available to assess the similarity of two curves, e.g. test and analytical acceleration responses. In this paper, average acceleration responses were calculated and simple percentage differences were obtained for the F-28 forward section only. This approach works well, but cannot provide a detailed assessment of the comparison. Time history responses could also be evaluated using the Roadside Safety Verification and Validation Program (RSVVP), which is a software program that automatically assesses the similarities of two curves as part of the validation process of a numerical model [30]. The program allows pre-processing of the two curves, including filtering, phasing, and timing adjustments, etc. Sixteen different metrics are included that are classified into 3 categories: (1) magnitude-phase-comprehensive (MPC) metrics, (2) single-value metrics, and (3) analysis of variance (ANOVA) metrics.

In past simulations, the MPC metric developed by Sprague and Geers [31], which provides a measure of the "goodness of fit" between two curves, was used. Three parameters are calculated over a specified time interval: Sprague and Geers Magnitude (SGM), Sprague and Geers Phase (SGP), and Sprague and Geers Comprehensive (SGC), which is a combination of magnitude and phase. Generally, a value of less than 40 for SGM, SGP, or SGC is considered passing the criteria. It is important to note that the magnitude and phase metrics are independent of one another. For example, if changes are made to the magnitude of one curve, but the phase information remains the same, only the magnitude metric will change, and visa versa. It should also be noted that if two identical curves are being compared, all three metric values would be zero. Consequently, metric values close to zero are desired. MPC metrics to assess time history comparisons could have been used in this model calibration effort. However, past experience has shown that the simple percentage difference approach may be a more stringent requirement. Consequently, the percentage difference approach was used.

C. ATD Response Prediction

It was previously noted that the acceleration response prediction of the seat/seat track interface for the F-28 wing-box section was greatly improved by replacing the concentrated masses with actual finite element representations of the seats and dummies. Concentrated masses do not accurately represent the load path provided by seated and restrained dummies. Consequently, a model was executed in which one row of seats were modeled, along with one LSTC Detailed FEM representing a Hybrid III ATD, and four rigid dummy torso blocks. However, predictions of dummy model pelvic acceleration responses for the F-28 wing-box section drop test were generally poor, even when a detailed occupant model was used that contained over 450,000 elements. The essential problem is that the ATDs and the ATD models are calibrated based on an automotive crash environment in which loading is primarily in the fore-aft direction. For this loading condition, head/neck flail and chest deflection are important. Consequently, the ATD models are calibrated to accurately predict this response. For crash loading conditions, the loading is primarily

in the vertical direction, which produces spinal compression and high lumbar loads. Unfortunately, the ATDs and the ATD models are not calibrated for this loading environment.

VII. CONCLUSIONS

In March 2017, a vertical drop test of a 10-ft.-long forward section of a Fokker F-28 aircraft was conducted as a part of a joint NASA/FAA effort to investigate the performance of transport aircraft under realistic crash conditions. Later, in June 2017, a drop test was performed on a 10-ft.-long wing-box section of the same F-28 aircraft. Both sections were configured with two rows of aircraft seats, in a triple-double configuration. A total of ten Anthropomorphic Test Devices (ATDs) were secured in the seats using standard lap belt restraints. In addition, both drop tests were conducted onto soil. The forward section was also configured with luggage in the cargo hold. The vertical drop of the forward section was conducted at 346.8-in/s. For the wing-box section test, the soil bed was canted by 10° facing downward. In addition, the wing-box section was pitched down by 2.9°. The measured impact velocity of the wing-box section was 349.2-in/s. This test configuration for the wing-box section was chosen to create an induced forward acceleration. Both drop tests were performed at the Landing and Impact Research facility located at NASA Langley Research Center.

A second objective was to assess the capabilities of finite element simulations to predict the test response. Finite element models were developed and executed in LS-DYNA®. The models contained accurate representations of the airframe structure, the hat racks and hat rack masses, the floor and seat tracks, the luggage in the cargo hold for the forward section, and the detailed under-floor structure in the wing-box section. Initially, concentrated masses were used to represent the inertial properties of the seats, restraints, and ATD occupants. However, later simulations were performed that included finite element representations of the seats, restraints, and ATD occupants. These models were developed to more accurately replicate the seat loading of the floor and to enable prediction of occupant impact responses.

Models were executed to generate analytical predictions of airframe responses, which were compared with test data to validate the model. Particular emphasis was placed on simulating seat track acceleration responses for both drop tests. Comparisons of predicted and experimental structural deformation and failures were made. Finally, predicted and experimental soil deformation and crater depths were also compared for both drop test configurations.

Major findings of this research are:

- For the F-28 forward section model with concentrated masses, analytical and experimental vertical acceleration and velocity responses were plotted for seven seat track locations. Average accelerations were determined for both the experimental and predicted responses and percentage differences were obtained. All of the percentage difference values are under

15%, indicating a good level of test/analysis agreement. Note that 5 of 7 data points are at or under 10%.

- For the F-28 forward section model with concentrated masses, the simulation predicted widespread failures of the center floor support structure, whereas the test article saw several discrete failures of the floor support beams and seat tracks. Both the test article and the model experienced plastic deformation and failures of the lower fuselage structure between the stanchions.

- For the F-28 forward section with concentrated masses, the simulation predicted a 0.14-in.-deep soil crater, while the actual crater measured between 0.15- and 1.75-in. in depth. This discrepancy was attributed to an extremely coarse mesh used in the soil model.

- For the F-28 forward section model that included physical representations of the seats and dummies, the simulation accurately predicted the impact sequence of events and occupant flailing. However, the pelvic acceleration responses for the ATD occupants on the double and triple aisle seats show acceleration magnitudes of 30-g for the double seat and 20-g for the triple seat. The model results indicate a much higher response, 40-g for the triple seat and 53-g for the double seat, with a sharper rise time (0.020-s) compared to the test data (0.050-s). Despite apparent reductions in the dynamic overshoot by incorporating changes based on several modeling factors, the ATD loads remained higher in the model compared with test.

- For the F-28 wing-box section model with concentrated masses, major findings from the test-analysis comparisons are that the model generally under predicted the magnitude of the measured vertical acceleration responses at seat/floor attachment locations. The overall shape and duration of the vertical acceleration responses were well predicted, despite the poor agreement in magnitude. Comparisons of the forward acceleration responses at these locations showed better overall agreement, with the exception that the model response often contained a sharp peak at 0.065-s that was not seen in the experimental data.

- In an effort to improve the test-analysis comparisons for the F-28 wing-box section, the model was updated to include a single row of seats, one LS-DYNA Detailed FEM model, and four additional rigid dummy torso blocks. Results of this simulation were much improved over the simulation using concentrated masses to represent the inertial properties of the seats and dummies.

- For the F-28 wing-box section model that included physical representations of the seats and dummies, the simulation accurately predicted the impact sequence of events and

occupant flailing. However, the pelvic acceleration results show acceleration magnitudes of 25-g for test and 45-g for the model.

- For the F-28 wing-box section, structural damage was limited to yielding and fracture of support beams in the lower cavity. The model predicted beam cross-sectional distortion, plastic yielding, and failure of beams in the lower cavity.

- Finally, the soil crater created by the wing-box section had a maximum soil depth of 8-in. measured at the initial impact location. Soil depths decrease with the distance away from the initial impact location. A fringe plot of z-displacement, taken near the end time of the simulation, shows a large amount of displacement (7.959-in.) at the point of section slap down. This behavior is not seen in the test; however, the overall shape of the soil deformation pattern matches the test response well.

VIII. ACKNOWLEDGEMENTS

The authors of this paper gratefully acknowledge the technician team at the LandIR facility for their hard work in configuring the test articles, adding instrumentation and the data acquisition systems, setting up cameras for collecting visual data, and preparing the test site. We would also like to thank Ms. Robin Hardy and her team for performing soil characterization testing. Finally, we would like to acknowledge Grace Vidlak, a summer intern, who performed many LS-DYNA simulations and generated numerous test-analysis comparison plots.

IX. REFERENCES

1. ***Federal Register***, Federal Aviation Administration, Aviation Rulemaking Advisory Committee, Transport Airplane and Engine Issues, Vol. 80, No. 214, November 5, 2015.

2. Vaughan V.L., Alfaro-Bou E., "Impact Dynamics Research Facility for Full-Scale Aircraft Crash Testing," NASA-TN-8179, April 1976.

3. Jones L. E., "Overview of the NASA Systems Approach to Crashworthiness Program," Proceedings of the American Helicopter Society 58th Annual Forum, Montreal Canada, June 11-13, 2002.

4. Lyle K. H., Stockwell A. E., and Hardy R. C., "Application of Probability Methods to Assess Airframe Crash Modeling Uncertainty," *Journal of Aircraft*, Vol. 44, No. 5, 2007, pp. 1568-1573.

5. Stockwell A. E., "Fokker F28 Fuselage Section Drop Test Simulation and Test/Analysis Correlation," Report No. SDSR-07RCG-093003, 2003, Lockheed Martin Company, Langley Program Office, Hampton, VA.

6. Williams M. S., and Hayduk R. J.,"Vertical Drop Test of a Transport Fuselage Center Section Including the Wheel Wells," NASA-TM-85706, 1983.

7. Fasanella E. L., and Alfaro-Bou E., "Vertical Drop Test of a Transport Fuselage Section Located Aft of the Wing," NASA-TM-89025, 1986.

8. Abramowitz A., Smith T.G, and Vu, T., "Vertical Drop Test of a Narrow-Body Transport Fuselage Section With a Conformable Auxiliary Fuel Tank Onboard," DOT/FAA/AR-00/56, 2000.

9. Logue T.V., McGuire R.J., Reinhardt J.W., and Vu T., "Vertical Drop Test of a Narrow-Body Fuselage Section with Overhead Stowage Bins and Auxiliary Fuel Tank System On Board," DOT/FAA/CT-94/116, 1995.

10. Abramowitz A., Smith T. G., Vu T., and Zvanya J., "Vertical Drop Test of an ATR 42-300 Airplane," DOT/FAA/AR-05/56, 2006.

11. McGuire R. J., Nissley W. J. and Newcomb J. E., "Vertical Drop Test of a Metro III Aircraft," DOT/FAA/CT-93/1, 1993.

12. McGuire R. J., and Vu T.,"Vertical Drop Test of a Beechcraft 1900C Airliner," DOT/FAA/AR-96/119, 1998.

13. Abramowitz A., Ingraham P. A., and McGuire R. J., "Vertical Drop Test of a Shorts 3-30 Airplane," DOT/FAA/AR-99/87, 1999.

14. Hallquist J. Q., "LS-DYNA Keyword User's Manual," Volume I, Version 971, Livermore Software Technology Company, Livermore, CA, August 2006.

15. Hallquist J. Q., "LS-DYNA Keyword User's Manual," Volume II Material Models, Version 971, Livermore Software Technology Company, Livermore, CA, August 2006.

16. Hallquist J. O., "LS-DYNA Theory Manual," Livermore Software Technology Company, Livermore, CA, March 2006.

17. Littell J. D., "A Summary of Results from Two Full-Scale F28 Fuselage Section Drop Tests," NASA Technical Memorandum, NASA/TM-2018-XXXXXX, 2018.

18. Littell J. D., "Large Field Photogrammetry Techniques in Aircraft and Spacecraft Impact Testing," Proceedings of the Society of Experimental Mechanics Annual Conference, Indianapolis, Indiana, June 7-10, 2010.

19. Littell J. D., "Experimental Photogrammetric Techniques used on Five Full-Scale Aircraft Crash Tests," NASA/TM-2016-219168, 2016.

20. Littell J. D., "Full Scale Drop Test of a Fokker F28 Forward Fuselage Section onto Soil," Aerospace Structural Impact Dynamics International Conference (ASIDI), Wichita, KS, October 17-19, 2017.

21. Thomas M. A., Chitty D. E., Gildea M. L. T'Kint C. M., "Constitute Soil Properties for Unwashed Sand and Kennedy Space Center." NASA CR-2008-215334, 2008.

22. Fasanella E. L., Jackson K. E., and Kellas S., "Soft Soil Impact Testing and Simulation of Aerospace Structures," Proceedings of the 10th International LS-DYNA Users Conf., Dearborn, MI, June 8-10, 2008.

23. American Society of Testing and Materials, "Standard Test Method for California Bearing Ratio (CBR) of Laboratory-Compacted Soils," ASTM-D1883, ASTM International, West Conshohocken, PA, 2016.

24. Jackson K. E. and Fasanella E. L., "Crash Simulation of Vertical Drop Tests of Two Boeing 737 Fuselage Sections," DOT/FAA/AR-02/62, 2002.

25. Jackson K. E., Fasanella E. L., Littell J. D., Annett M. S. and Stimson C. M., "Simulating the Impact Response of Three Full-Scale Crash Tests of Cessna 172 Aircraft," NASA Technical Memorandum, NASA/TM–2017-219599, July 2017.

26. Guha, S., "LSTC_NCAC Hybrid III 50th Dummy – Positioning and Post-Processing," Livermore Software Technology Company (LSTC Michigan), May 29, 2014.

27. Society of Automotive Engineering, J211-1 Instrumentation for Impact Test – Part 1 Electronic Instrumentation, Revision March, SAE International, 400 Commonwealth Drive, Warrendale, PA, 1995.

28. Fasanella E. L. and Jackson K. E., "Best Practices for Crash Modeling and Simulation," NASA TM-2002-211944, ARL-TR-2849, 2002.

29. Lyle K. H., Bark, L. W., and Jackson, K. E., "Evaluation of Test/Analysis Correlation Methods for Crash Applications," ***Journal of the American Helicopter Society***, Vol. 47, No. 4, pp. 219-232, 2002.

30. Mongiardini M., Ray M. H., Anghileri M., "Development of a Software for the Comparison of Curves During the Verification and Validation of Numerical Models," Proceedings of the 7th European LS-DYNA Conference, Salzburg, Austria, 2009.

31. Sprague M.A. and Geers T. L., "Spectral Elements and Field Separation for an Acoustic Fluid Subject to Cavitation," ***Journal of Computational Physics***, Vol. 184, 2003, pp: 149-162.

REPORT DOCUMENTATION PAGE

Form Approved
OMB No. 0704-0188

1. REPORT DATE *(DD-MM-YYYY)*
01-02-2018

2. REPORT TYPE
Technical Memorandum

3. DATES COVERED *(From - To)*

4. TITLE AND SUBTITLE

Finite Element Simulations of Two Vertical Drop Tests of F-28 Fuselage Sections

5a. CONTRACT NUMBER

5b. GRANT NUMBER

5c. PROGRAM ELEMENT NUMBER

6. AUTHOR(S)

Jackson, Karen E.; Littell, Justin D.; Annett, Martin S.; Haskin, Ian M.

5d. PROJECT NUMBER

5e. TASK NUMBER

5f. WORK UNIT NUMBER
664817.02.07.03.03

7. PERFORMING ORGANIZATION NAME(S) AND ADDRESS(ES)

NASA Langley Research Center
Hampton, VA 23681-2199

8. PERFORMING ORGANIZATION REPORT NUMBER
L-20895

9. SPONSORING/MONITORING AGENCY NAME(S) AND ADDRESS(ES)

National Aeronautics and Space Administration
Washington, DC 20546-0001

10. SPONSOR/MONITOR'S ACRONYM(S)
NASA

11. SPONSOR/MONITOR'S REPORT NUMBER(S)
NASA-TM-2018-219807

12. DISTRIBUTION/AVAILABILITY STATEMENT

Unclassified
Subject Category 39
Availability: NASA STI Program (757) 864-9658

13. SUPPLEMENTARY NOTES

14. ABSTRACT

In March 2017, a vertical drop test of a forward fuselage section of a Fokker F-28 MK4000 aircraft was conducted as part of a joint NASA/FAA project to investigate the performance of transport aircraft under realistic crash conditions. In June 2017, a vertical drop test was conducted of awing-box fuselage section of the same aircraft. Both sections were configured with two rows of aircraft seats, in a triple-double configuration. A total of ten Anthropomorphic Test Devices(ATDs) were secured in seats using standard lap belt restraints. The forward fuselage section was also configured with luggage in the cargo hold. Both sections were outfitted with two hat racks, each with added ballast mass. The drop tests were performed at the Landing and Impact Research facility located at NASA Langley Research Center in Hampton, Virginia. The measured impact velocity for the forward fuselage section was 346.8-in/s onto soil. The wing-box section was dropped with a downward facing pitch angle onto a sloping soil surface in order to create an induced forward acceleration in the airframe. The vertical impact velocity of the wing-box section was 349.2-in/s. A second objective of this project was to assess the capabilities of finite element simulations to predict the test responses.

15. SUBJECT TERMS

Explicit transient dynamic; Finite element modeling; LS_DYNA; Nonlinear; Regional jet aircraft

16. SECURITY CLASSIFICATION OF:			17. LIMITATION OF ABSTRACT	18. NUMBER OF PAGES	19a. NAME OF RESPONSIBLE PERSON
a. REPORT	b. ABSTRACT	c. THIS PAGE			STI Help Desk (email: help@sti.nasa.gov)
U	U	U	UU	71	19b. TELEPHONE NUMBER *(Include area code)* (757) 864-9658